



MUNICH INSTITUTE OF ROBOTICS AND MACHINE INTELLIGENCE

TECHNICAL UNIVERSITY OF MUNICH

Bachelor's Thesis in Electrical Engineering

An Automated Experimental Setup for the Evaluation of Tactile Sensors for Robotic Hands

Manuel Krummschmidt





MUNICH INSTITUTE OF ROBOTICS AND MACHINE INTELLIGENCE

TECHNICAL UNIVERSITY OF MUNICH

Bachelor's Thesis in Electrical Engineering

An Automated Experimental Setup for the Evaluation of Tactile Sensors for Robotic Hands

Ein automatisierter Versuchsaufbau für die Bewertung
von taktilen Sensoren für Roboterhände

Author: Manuel Krummschmidt
Supervisor: Prof. Dr.-Ing. Sami Haddadin
Advisor: M.Sc. Sonja Gross
Submission Date: May 09, 2022

I confirm that this bachelor's thesis is my own work and I have documented all sources and material used.



München, May 09, 2022

Manuel Krummschmidt

Abstract

Despite the fact that the designs of modern tactile sensors are often based on the same physical principles, the testing methods for tactile sensors are not uniform. Thereby it is necessary that the sensors are evaluated with the same test methods to enable the comparison of different sensor designs.

The aim of this thesis is to develop an automated experimental setup that is able to reliably conduct the methodologies necessary for characterizing and evaluating tactile sensors in a structured manner. These include the testing of normal and shear forces as well as vibration within linear, dynamic and static experiments.

The requirements for the experimental setup are derived from the requirements for tactile sensors in manipulation. Thereby the system utilizes a Franka Emika Panda Robot as an actuator to apply forces to the sensors. A 3-axis force sensor is mounted at the end effector to collect reference data during experiments. Thereby the force is applied through a probe attached to the sensor. Two mounting structures are designed and 3D printed to fixate the tactile sensors. A control system based on Python and MIOS is implemented for robot control. The setup is evaluated regarding its ability to reliably carry out the designed experiments. Thereby a maximum target force deviation of 10 % is allowed to meet the requirement.

It is concluded that none of the designed experiments meet the threshold for any experiment variation. Linear, dynamic cyclic and quasistatic cyclic experiments show a maximum deviation of the target force F_z of 13.9% ($F_t = 10N$), 493% ($F_t = 1N$) and 5.10% ($F_t = 10N$) respectively. In addition, unintended shear forces are observed for every normal force experiment.

Shear force experiments XY (F_y in xy-plane) and XYZ ($F_{x,y} \& F_z$) show a maximum deviation of the target force of 1.6% ($F_t = 5N$) and 0.6% ($F_{t,x} = 3N$), 0.6% ($F_{t,y} = 3N$) and 89,9% ($F_t = 5N$). A sliding experiment is conducted that shows a maximum deviation of the target force of 26% ($F_t = 1N$)

Reasons for these deviations are a delay between the measurement of the force target and the corresponding actuator reaction, as well as an unintended movement of the end effector for movements with x and z components.

Additionally to the movement uncertainty, a measuring uncertainty of the sensor of 0.05N to 0.1 N and a shear force bias for XY experiments of about 0.07N is observed.

Further optimization is required so that the experimental setup is usable for sensor characterization and evaluation.

Contents

Abstract	III
1. Introduction	1
2. State of the Art	2
2.1. Introduction to Tactile Sensors	2
2.1.1. Tactile Sensing and its Applications	2
2.1.2. Sensor Characteristics and Requirements	4
2.2. Evaluation of Tactile Sensors	7
2.2.1. Sensor Calibration	7
2.2.2. Static and Dynamic Evaluation	8
2.3. Experimental Setups	9
2.3.1. Experimental Setups utilizing Robots	12
2.3.2. Reliability measures for Experimental Setups	13
3. The Automated Test Setup	16
3.1. Concept Development	16
3.1.1. Setup Requirements	16
3.1.2. Experiment Design	18
3.1.3. System Concept	20
3.2. Hardware Implementation	25
3.3. Software Implementation	26
4. Evaluation	28
4.1. Results	29
4.2. Discussion	39
5. Conclusion and Outlook	48
6. References	50
A. CAD Drawings	54

1. Introduction

The human sense of touch plays a vital role in how humans perceive their environment [Dah+10]. It allows us to distinguish between different materials, feel the temperature of objects, regulate grip strength and perform fine motor tasks [DV13].

For more than 50 years, scientists have been conducting research to replicate this ability into an artificial sense of touch [LL86]. The result of this research are tactile sensors - instruments that transduce tactile information into electrical signals. This technology has since been embedded into a multitude of technologies [LL86].

In prosthetics, this technology is utilized for hand prostheses that provide tactile feedback and make the amputees feel like it is part of their body rather than a tool [JF14]. For robotic applications, tactile sensors are embedded into artificial dexterous hands to enable a more autonomous generation of robots that is capable of operating in unstructured environments [Kap+15].

Currently, a team of researchers at the Munich Institute of Robotics and Machine Intelligence (MIRMI) is working on the development of a robotic hand. In the scope of this project, they develop tactile sensors with the aim to implement them into the hand design. These tactile sensors are based on different principles such as barometric pressure, capacitive, piezoresistive, piezoelectric or the hall-effect.

To determine which sensor design is best suited for the task, the sensor designs are compared. For this, the same testing methodologies are executed on the tactile sensors to enable the comparability between the different designs. Therefore they are evaluated regarding the measurement of normal forces, shear forces and vibration. The methods applied are sensor characterization, dynamic cyclic, quasistatic cyclic testing and sliding.

The aim of this thesis is to develop an experimental setup that is able to reliably conduct the methodologies necessary for characterizing and evaluating tactile sensors. Thereby the experiments are executed in a structured manner to allow for a comparison of different designs.

First, the requirements for the experimental setup are formulated based on the guidelines for tactile sensors in manipulation tasks and testing methods. From this, a system concept and experiment procedures are developed.

Next, the software and hardware components are implemented and combined into the final setup. Subsequently, the experimental setup is evaluated regarding its capability to execute the required methodologies and measure the applied forces within the formulated requirements. Thereby the experiment results are presented, discussed and possible improvements are outlined.

2. State of the Art

2.1. Introduction to Tactile Sensors

2.1.1. Tactile Sensing and its Applications

Tactile sensing technology provides an artificial equivalent to the human sense of touch [Dah+10]. It enables the detection of mechanical contact properties with the environment like location, magnitude and angle of contact forces as well as vibration at the point of contact [Li+20]. Thereby the contact forces consist of a normal and tangential component (figure 2.1). These modalities give insight into shape, hardness or texture of a surface [Dah+10] as well as interactions like contact or sliding [LL86]. Tactile sensing may also provide information about thermal properties of a material [Li+20], however this aspect is not covered in this thesis.

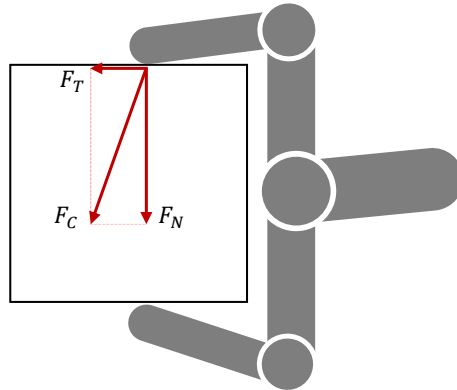


Figure 2.1.: A visual representation of contact force. A force F_C is exerted onto an object during grip. It is composed of a normal force F_N perpendicular and a tangential force F_T parallel to the object surface.

According to Cutkosky et al., the task domains of robots that make use of this information can be divided into three categories: manipulation, exploration and response (figure 2.2) [CHP07].

Manipulation tasks involve object grasping, In-Hand-Manipulation (rearranging of an objects orientation in grasp) or nonprehensile manipulation (object manipulation without grasping) [Li+20].

The grasp stability is dependent on contact parameters such as the local object geometry, magnitude and direction of contact force and friction at the point of contact [Li+20]. Thereby tactile sensing provides insight on this information and helps to improve grasp stability [Li+20]. This is demonstrated by Wettels et al. who implemented dynamic grip force control with a

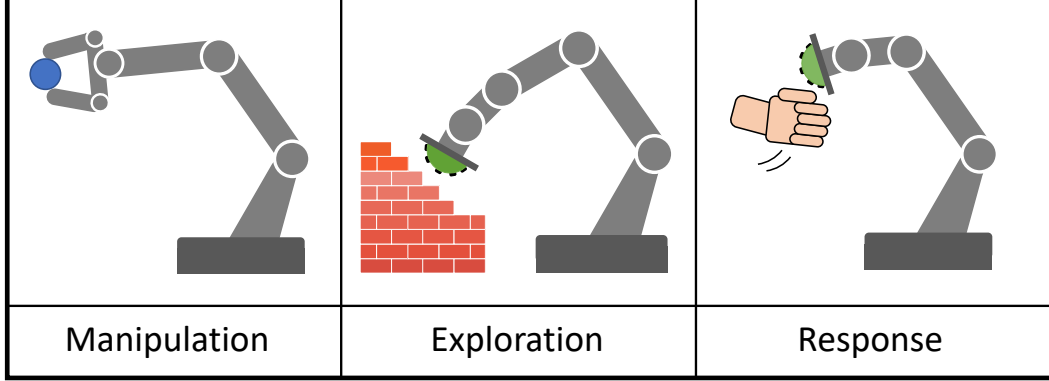


Figure 2.2.: Different categories of tactile sensing in robotics. Adapted from [CHP07].

biomimetic tactile sensor attached to a robotic hand. Here, the tactile sensor provides measurements of the contacts tangential forces. Thereby a sudden increase in tangential forces indicates that the object is sliding out of the grip. This serves as cue to increase grip force [Wet+09]. Morales et al. utilized tactile sensors mounted on the fingertips of a robotic hand to optimize the contact area of a grasp. Thereby the tactile sensors generate tactile images that provide information on the quality of the initial contact. If the contact area is too small, the appropriate motion is executed to maximize the contact area [Mor+07].

[Su+15] further demonstrate the importance of grip force control for handling fragile objects. Thereby the grip force has to be adjusted appropriately to avoid damaging the objects (figure 2.3 (a)). This shows that the ability to monitor contact properties is beneficial for a robots capability of handling various objects [Li+20].

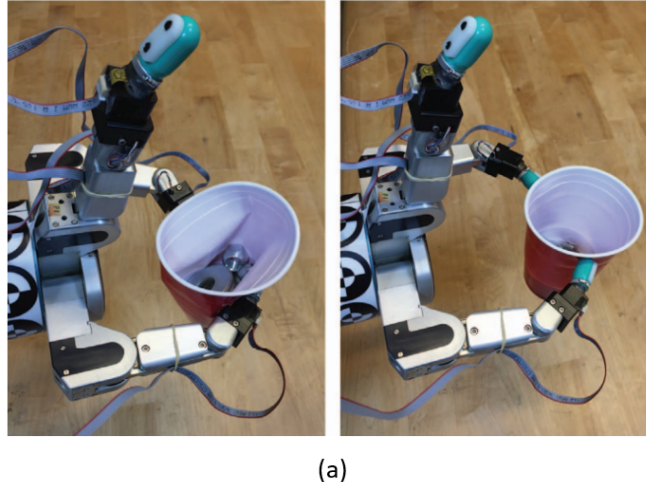


Figure 2.3.: A robotic hand equipped with a biomimetic sensor. Adaptive grip control for delicate objects. Adapted from [Su+15].

Exploration tasks aim to obtain information about object properties. Touching or sliding over a surface generates tactile data such as force distribution, friction or vibration which is used to determine shape, hardness or surface texture [DV13]. This allows differentiation between objects [DV13].

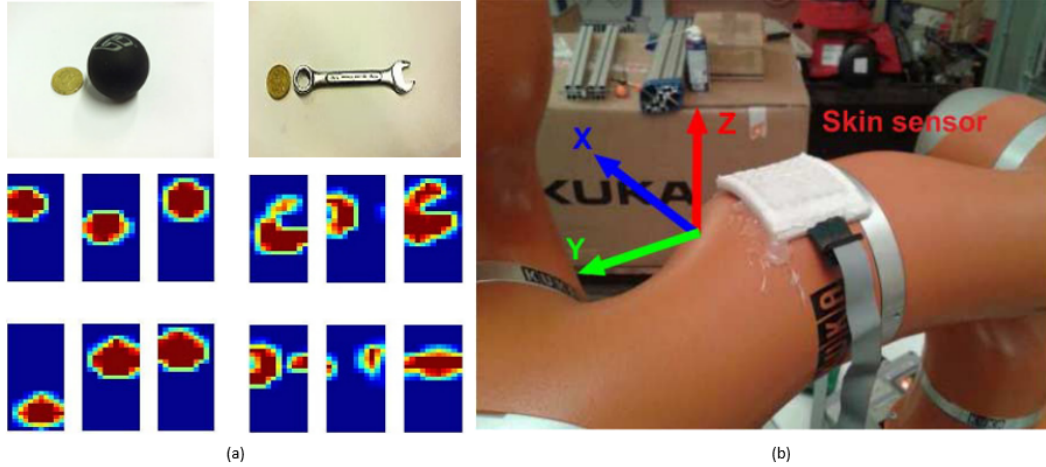


Figure 2.4.: Applications for tactile sensors in exploration and response tasks. (a) Object identification through tactile pressure maps [Liu+15]. (b) Tactile sensor skin mounted on a robot [Cir+16]

Liu et al. (2012) determined the friction-coefficient and texture of different surfaces by using classification algorithms on force and vibration data collected from sliding a finger-shaped tactile sensor along object surfaces at variable velocities.

Figure 2.4 (a) shows tactile images generated by repeatedly touching a ball and a wrench with a tactile sensor array. These tactile images are used to train a supervised learning algorithm that is able to distinguish different objects by shape [Liu+15].

The ability to obtain tactile information of the environment enables robots to operate in unstructured environments and therefore increases their autonomous capabilities [DV13].

Response tasks involve detecting contacts between the robot and external influences.

Here, key elements are detecting external contact, measuring the forces and reacting appropriately [CHP07]. For this, flexible skin-like tactile sensors are utilized. They are made out of soft, compliant materials that enable mounting to various surface structures [RZM21].

Cirillo et al. presented a flexible sensor array that is able to accurately measure contact location and force, while providing the necessary flexibility for mounting on a robot. Figure 2.4 (b) shows a robot equipped with the artificial skin [Cir+16]. This application important for tasks in physical human-robot interaction (pHRI), where safety is a major concern [Had14].

To provide a better understanding for tactile sensors, the following section introduces general sensor characteristics and the requirements for sensors in manipulations tasks.

2.1.2. Sensor Characteristics and Requirements

The sensor characteristics are defined by the physical abilities and limitations of the sensor [Fra16]. They are used to evaluate general sensor performance and indicate if a sensor meets the requirements for specific tasks [Reg12]. Some of the most important sensor characteristics are described by [Fra16]:

The **Transfer function** is a mathematical description of the relationship between physical

input and electrical output signal.

Sensitivity is defined as the slope of the transfer function. It describes how much a change in the input signal affects the output signal. This is shown in figure 2.5 (a) where two transfer functions with different slopes are indicated.

Accuracy reflects the error of measurement. It is defined as the difference between a measured value and the true value of the input signal.

Dynamic Range defines the span (minimum and maximum) of input signals that may be converted to electrical signals.

Resolution defines the smallest detectable variation of the input signal.

Nonlinearity describes to which extent the measured transfer function deviates from the ideal straight line. Figure 2.5 (b) depicts the ideal curve of a sensor and the real curve.

Saturation occurs when a sensor measures a value outside of its dynamic range. As seen in figure 2.5 (c), upon reaching saturation, the slope of the transfer function reaches towards zero .

Response time indicates the time needed for the sensor output to reach a new state after a change of input.

Short-term drift (Instability) describes the change in output signal within a short time span (minutes to days) independent from input.

Long-term drift is caused by physical changes of sensor properties over a long time span and produces a permanent change in the output signal.

Hysteresis describes the difference of output values at any measurement point when approaching the point by increasing or decreasing the input signal (figure 2.5 (d)).

Material properties such as conductivity, robustness and compliance also impact sensor performance [Reg12].

The requirements for tactile sensors vary based on whether it is intended for manipulation, exploration or response applications. This thesis will focus on the requirements for manipulation tasks.

Requirements for Tactile Sensors in Manipulation

General specifications for tactile sensors used in manipulation tasks are depicted by [Har82], [DN04] and [Dah+10].

The contact between a robot gripper and objects occur with varying force magnitudes and at different locations. Therefore normal and shear forces during grasp as well as their directions are required to be detectable. Here, a range of 0-10 N is desirable for everyday objects [Har82] [DV13]. When handling light objects a high force resolution is required to detect small changes in contact force. For this, a resolution of 0.01 N to 0.1 N is deemed useful [Har82] [DN04].

For contact point estimation during object manipulation, a high spatial resolution is desirable [Kap+15]. Thereby the spatial resolution of a tactile sensor should be between 1-2 mm if it is utilized as fingertip [Har82] [DN04].

Furthermore, a tactile sensor should exhibit a frequency response of at least 100 Hz for vibration sensing and response times [Har82] [DN04]. Moreover, Harmon states that low hysteresis and linearity are desired, as sensor behaviour is preferred to be stable, monotonic and repeatable. In addition to the sensing requirements, tactile sensors should be resilient to wear and tear and withstand harsh environment conditions to avoid sensor degradation over time [Dah+10].

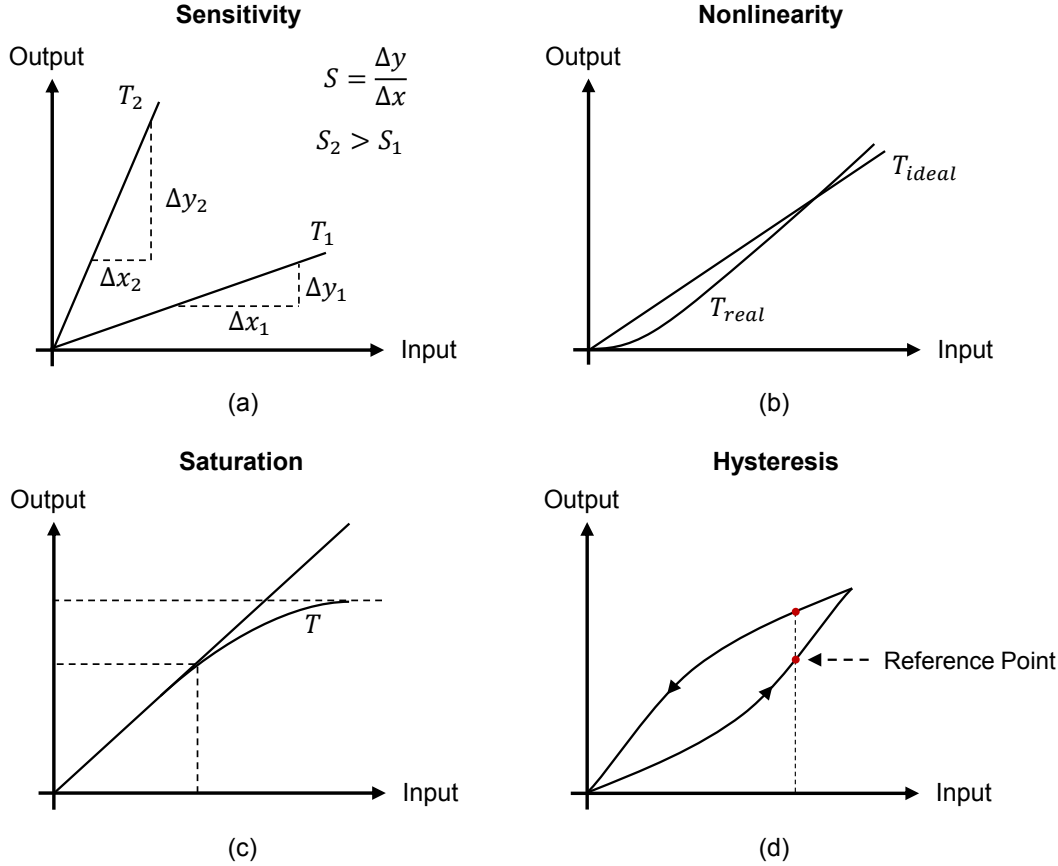


Figure 2.5.: Visualization for various sensor characteristics. (a) Sensitivity. (b) Nonlinearity. (d) Saturation. (d) Hysteresis. Adapted from [Fra16].

Thereby they are desired to be soft and flexible for attachment to various 3D structures [Dah+10]. Additionally, the sensors should have a compliant structure [DV13]. First, it provides more contact information through the increase of surface area under deformation [DV13]. And second, a soft surface enables handling of fragile objects without damaging them [Su+15].

Further requirements include resistance to electromagnetic interference in close proximity [Yin+18], low manufacturing costs [Har82] and miniaturizeability for better integration [Sch+10]. A summary of the most important requirements can be found in table 2.1

During the development of a tactile sensor, these characteristics should be determined to gain insight on the sensor behaviour. The required experimental methodologies and setups are depicted in the following.

	Requirements
Modalities	Normal & Shear Forces, Vibration
Force range	0 - 10 N
Force Resolution	0.01 N - 0.1 N
Frequency Response	At least 100 Hz
Spatial resolution	0.1 - 2 mm
Sensor response	Low hysteresis, linear, monotonic, stable, repeatable
Material	Soft, flexible, compliant

Table 2.1.: Summary of requirements for tactile sensors for manipulation tasks. [Har82], [DN04], [Dah+10]

2.2. Evaluation of Tactile Sensors

2.2.1. Sensor Calibration

The aim of sensor calibration is to find the best approximation for the relationship between the physical input stimulus and the electrical output signal of the sensor [Fra16].

In this process, the reference data recorded during the experiments is used to approximate the transfer function via curve fitting [Fra16]. Thereby the calibration accuracy is limited by the accuracy of the reference data [Fra16].

The parameters of the transfer function are adjusted such that the function fits the reference data using e.g. linear or polynomial functions [Fra16]. This is shown in figure 2.6 where linear and polynomial functions are used to approximate the sensor response [KSA15]. Further information can be found in [Fra16].

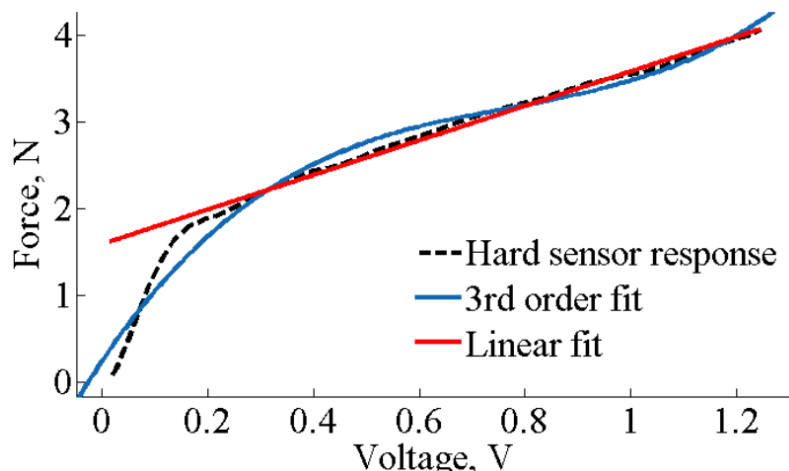


Figure 2.6.: Example for approximating a transfer function with a linear and polynomial approach. Adapted from [KSA15]

2.2.2. Static and Dynamic Evaluation

Generally, there is no uniform list of procedures for evaluating a tactile sensor. However, static and dynamic testing methods provide data that enable sensor characterization [Zhu+20] [GSC20] [Jam+15] [KSA15] [Wan+16].

Linear force loading generates data for sensor calibration [Zhu+20] [KSA15]. This process is depicted in figure 2.7 (a). Linear forces are loaded to a target force and released at the same rate. The sensor response to the monotonous force provides insight into the relationship between physical input and sensor signal [Fra16].

Thereby sensor characteristics such as the transfer function, sensitivity, dynamic range, resolution and nonlinearity of the sensor are determined [Jam+15] [Lee+08] [Wan+16].

Examples for sensor calibration on tactile sensors can be found in [Jam+15], [Noh+16], [Wan+16] and [Zhu+20].

Dynamic cycle testing is executed to gain insight on characteristics such as hysteresis, response time, signal repeatability and dynamic signal drift [GSC20] [Zhu+20].

As depicted in figure 2.7 (b), the sensors must endure force loading cycles of different magnitudes within quick succession at variable frequencies. Thereby the procedure reveals if the sensor signal shows a deviation from the expected response in between the cycles [GSC20] [Zhu+20]. This test can also reveal material deficiencies such as permanent deformation through load and is thus also suitable for determining sensor robustness [GSC20].

Quasi-static cycle is used to determine the sensor drift during static load periods [Zhu+20] [Jam+15] [GSC20].

In this process, static forces are applied as depicted in figure 2.7 (c). Thereby the applied forces are held constant for a dwell time t_1 and the different cycles are separated by a pause. This procedure reveals if the sensor signal shows a drift during the dwell time [GSC20]. The pause allows the sensor material to regain shape after deformation [GSC20].

Methods not included in this thesis are testing the influence of temperature on the sensor signal [Tom+16] and observing the sensor response to a high frequency sinusoidal force [BK18] [Zhu+20].

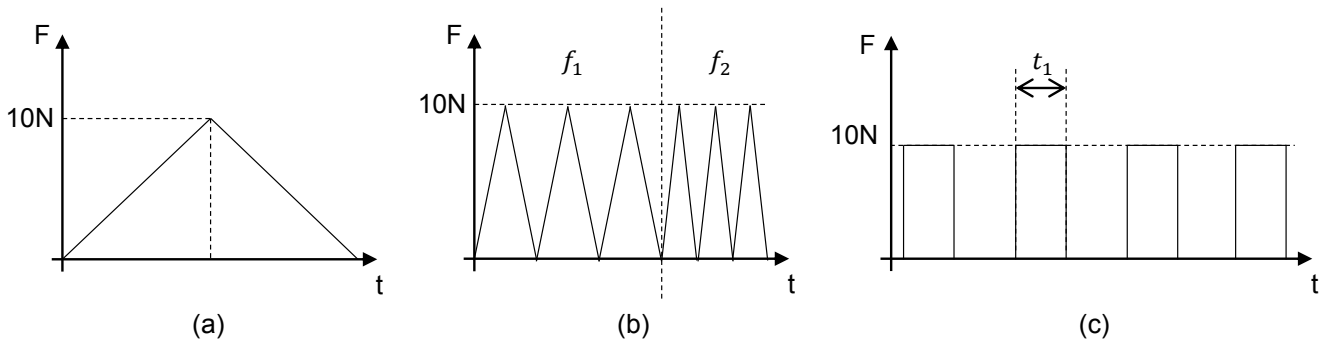


Figure 2.7.: Force graphs for different testing methods. (a) Linear force loading for sensor calibration. (b) Dynamic cycle testing to examine the dynamic response of a sensor. (c) Quasi-static cycle testing to determine sensor drift.

2.3. Experimental Setups

Experimental setups are required to evaluate the characteristics of a tactile sensor. They enable controlled empirical measurements that show the sensor response to different modalities such as normal and shear forces or vibration. Thereby it is determined to what extent a sensor is capable of measuring a certain modality. This chapter describes the overall structure of experimental setups throughout the literature.

In general, an experimental setup consists of an actuator to apply forces, a sensor for measuring reference force data and a mounting structure for the tactile sensors. Thereby the structure varies depending on which modality is tested.

Normal and Shear Forces

A sensors capability to detect normal and shear forces is generally tested by deforming the sensor surface with a sensor probe [YSP17] [Yua+15] [Tom+16]. Their size depends on the type of sensor and they have various shapes such as rectangular, round, spherical or angled [PPS12] [YSP17] [Yua+15] [Tom+16]. Thereby the methods of how forces are actuated throughout the literature are similar but not uniform.

In various setups, the actuation is done manually. Thereby a force is applied through weights [PPS12]. Figure 2.8 (a) depicts an example for this type of setup [PPS12]. A load platform is connected to a flat, rectangular probe positioned above a single taxel of a tactile sensor. During experiments, masses of 250g in total are added step-wise to the platform, increasing normal force with a constant increment to indent the sensor surface [PPS12]. Additionally, [Nod+09] demonstrate that it is viable to apply shear force with this method. As shown in figure 2.8 (b) a wire is attached to a plate positioned beneath the tactile sensor. While the sensor is fixed through a weight placed on top of it, shear stress is applied through weights pulling on the wire [Nod+09]. Although this is a straightforward method of applying forces, [PPS12] and [Nod+09] show that the possible force resolution is limited by the available weights. This is solved by using a mechanical actuator described in the following.

Multiple experimental setups utilize linear stages as actuators. They enable the positioning of a probe with a high spatial accuracy (0.01 mm in [Yua+15], 100 nm in [Lee+08], 0.5 μ m in [Wan+16]). With this, the forces are applied with a high resolution [Wan+16] [Lee+08]. Thereby the stages are mounted in a vertical or horizontal position.

To apply normal forces on to a tactile sensing array, [Ji+16] uses a vertically mounted, one-dimensional linear stage. Whereas [Noh+16] displays a different approach that uses a single one-dimensional linear stage for both normal and shear force testing. Thereby a horizontal linear stages drives a sensor probe into the sensor surface. For normal force, the tactile sensor is mounted in parallel to the sensor probe (figure 2.8 (d, upper)), while for shear force the sensor is mounted vertically and is connected to the probe via a wire (figure 2.8 (d, lower)).

This shows that linear stages serve as an accurate actuator. However, a one-dimensional linear stage restricts the movement to a single translational force at a time. This is a problem for experiments where normal and shear forces are required at the same time. An example for this is the determination of crosstalk, where the influence of different force axes on each other is investigated [Wan+16]. A common solution for this is to combine multiple linear stages to one multi-dimensional actuator.

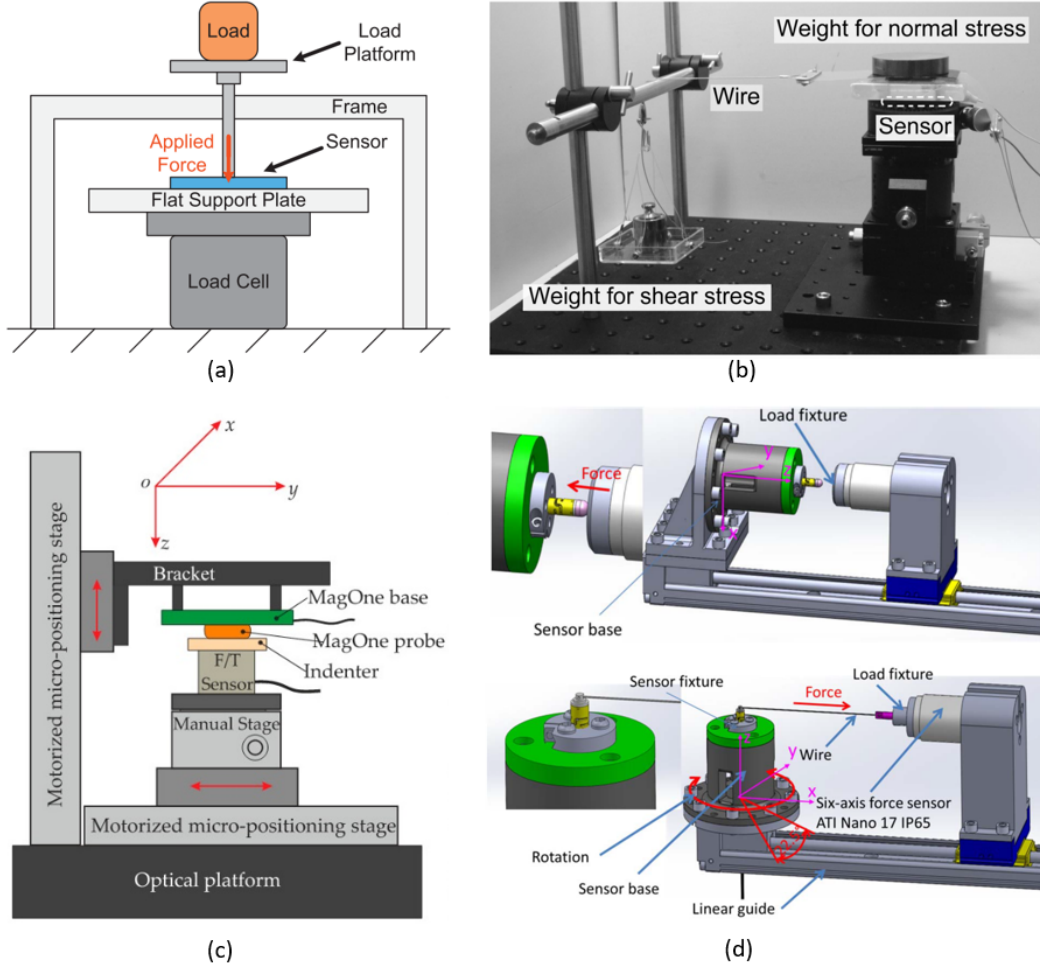


Figure 2.8.: Experimental setups with two types of actuators. (a), (b) Utilize weights to apply forces on tactile sensors [PPS12] [Nod+09]. (c), (d) Use linear stages to drive a probe into the sensor surface [Wan+16] [Noh+16].

The combined movement of several linear stages allows movements in multiple directions. With this, normal and shear forces can be applied simultaneously [Wan+16] [Yua+15]

For example, [Yua+15] mounted a GelSight sensor to a rotational stage and used a two-dimensional stage to actuate the sensor probe. Here the 2D stage enables testing of normal and shear forces, while the rotational stage can additionally be used to apply a rotational force component.

Similarly, [Wan+16] constructed a 3D actuator with three linear stages; two motorized and one manual (figure 2.8 (c)). While the manual stage is used to adjust the position of the tactile sensor, the other stages are used to drive the probe into the sensor surface. This setup is utilized to conduct experiments where both normal and shear forces are applied at the same time [Wan+16]. Thereby it is possible to adjust the applied forces individually to test different contact configurations [Wan+16]. This demonstrates the advantage of utilizing multiple linear stages at once.

Furthermore, linear stages may be used to apply forces from different angles. This is shown by [Tom+16], who used a rotatable sensor mounting plate in combination with corresponding angled probes. Figure 2.9 (a) shows the platform which is adjustable to various angles. With

this structure, forces are applied to the sensor surface from variable directions utilizing a single vertically mounted linear stage.

Similarly, [ACP17] used probes shaped with various surface angles. A 45° angled probe is shown in figure 2.9 (b), which is used to evaluate the tactile sensors capability to estimate the orientation of the surface.

This shows that utilizing linear stages in combination with various probes and adjustable mounting structures enables throughout testing of tactile sensors regarding normal and shear forces.

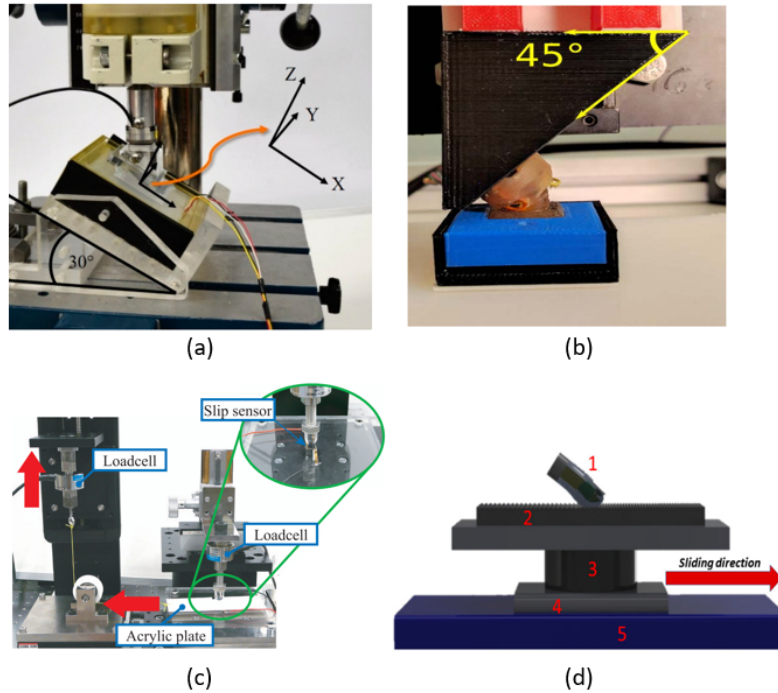


Figure 2.9.: Experimental setups for shear force and sliding. (a) Uses an adjustable sensor mount and angled probe to test from different angles [Tom+16]. (b) Utilizes probes with different angles [ACP17]. (c), (d) Create a sliding motion on the sensor surface with linear stages [Tes+09] [Rom+17].

Vibration

Experimental setups for testing a tactile sensors capability to detect vibration focus on the motion of a probe. Thereby a sliding motion across the sensor surface is executed to induce a vibration signal [Tes+09][Rom+17]. This is realized with linear stages. Figure 2.9 (c) shows a double linear stage setup for this purpose. Thereby one linear stage is used to pull on a plate mounted beneath the sensor, while the second stage applies a normal force. During this motion, the sliding plate creates measurable vibrations on the sensor surface that are used to detect slippage. With this configuration, various contact forces and sliding velocities can be tested. [Tes+09]. In this setup, the sensor is fixed through the applied normal force.

Similarly, [Rom+17] mounted the tactile sensor in a fixed position and moved the contact surface beneath. Thereby one linear stage moves the surface beneath the sensor horizontally and the other pushes the surface into the sensor with a defined contact force. As depicted in figure 2.9 (d)), this creates a sliding motion where the sensor records vibrations caused by grooves on the

plate surface [Rom+17]. Within these setups, the linear stages allow a controlled movement in horizontal direction while contact forces can be adjusted variably. Different setups for vibration testing are depicted later in this chapter.

Reference Data and Sensor Mounting

Additionally to the actuator, experimental setup utilize measuring instruments for recording force reference data and different methods to mount the tactile sensors.

Load cells or six-axis force/torque sensor are utilized for force sensing. Thereby the instruments are mounted in different configurations. This is shown in figure 2.8 (a) & (c) where [PPS12] and [Wan+16] use force sensors positioned statically beneath a plate. Similarly, figure 2.8 (d) and 2.9 (c) show how [Noh+16] and [Tes+09] attach their force sensing instrument behind the probe. In both cases, the positioning of the device allows the applied forces to be recorded during experiments.

The tactile sensors are mounted with various methods. For example, an adhesive strip [PPS12] or metal weights [Tes+09] can be utilized to secure the sensor. In some setups, a custom designed mounting bracket is required [Wan+16] [ACP17]. Here it is viable to either mount the sensor statically [Noh+16] or on the actuator [Wan+16]. Thereby the mounting structures are intended to fixate the sensor to prevent any unintended movement during force loading.

This shows that experimental setups display varying structures based on the modality that is to be tested. A different type of experimental setup that utilizes robots is introduced in the following.

2.3.1. Experimental Setups utilizing Robots

Collaborative robots (cobots), are a generation of robots that enable new applications in physical Human-Robot Interaction (pHRI) [Had14]. In contrast to conventional industrial robots that are mounted within safety cages, cobots are equipped with safety mechanisms that allow for them to be operated in close proximity to humans [Had14]. These mechanisms include algorithms for detecting unintentional collisions or deliberate interaction [Had+08].

Consequently, this enables researchers to utilize cobots as actuators for their experimental setups. Commonly used are the KUKA LBR [KUK22] and the UR5e [Rob22] due to their lightweight design and their ability to move their end effector within six and seven degrees of freedom, respectively [Pia+20] [JPL18]. Thereby they are used for normal/shear force and vibration testing.

Their capability for force testing is demonstrated by Piacenza et al. who used a UR5e robot arm in combination with a linear stage. Figure 2.10 (a) shows the linear stage mounted on a custom end effector. Thereby it is oriented freely around the tactile sensor and indent the surface from various angles [Pia+20]. To measure the applied forces, a force sensor is mounted behind the probe. This combines the dynamic movement capabilities of a robot arm with the accuracy of a linear stage.

For vibration testing, the tactile sensor are mounted to the end effector of a robot. This is shown in figure 2.10 (b), where Romeo et al. attached a bioinspired tactile sensor to a robotic hand mounted on a KUKA robot. Thereby the robot executes a motion that slides the sensor

across different surfaces. During this movement, the tactile sensor measures vibrations in the friction force. This data is used to indicate slippage [Rom+21]. This setup thereby tests the sensor at velocities of up to 8 cm/s with various contact forces [Rom+21].

It is demonstrated that experimental setups are utilized to test the capability of a tactile sensor to detect normal/shear forces and vibration. The modalities are tested manually, with linear stages or cobots. For the characterization of the tactile sensors, reference force data is collected with force sensors.

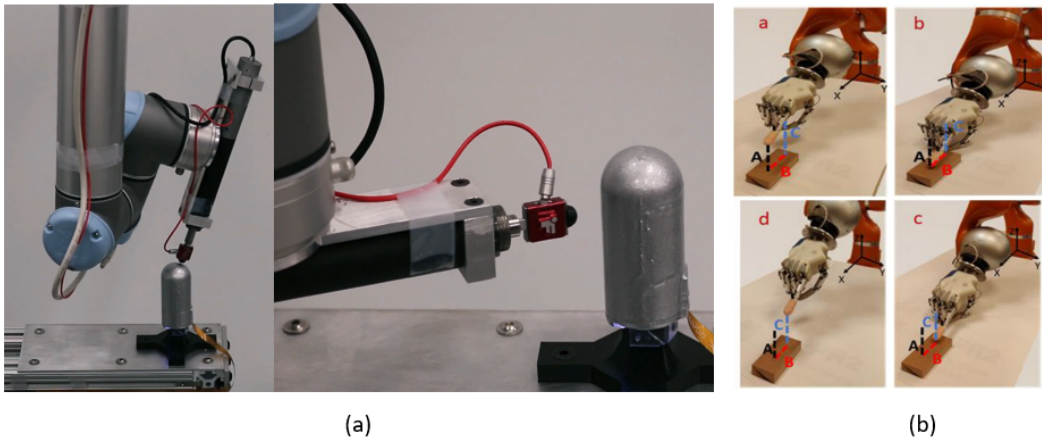


Figure 2.10.: Experimental setups utilizing robots. (a) Shows a UR5e robot with a linear stage mounted at its end effector [Pia+20]. (b) Shows a KUKA LBR robot sliding a biomimetic tactile sensor over a surface [Rom+21]

Within this thesis, an experimental setup utilizing a Franka Emika Panda robot [Emi22] as actuator is developed. To determine if this setup produces appropriate results, the setup is evaluated in section 4. Therefore the necessary measurement terms are introduced in the following.

2.3.2. Reliability measures for Experimental Setups

As shown in the previous section, an experimental setup is used for both applying and measuring forces. According to [Fri12], every measurement of a physical quantity is subjected to errors. These can be categorized into two main types of measurement errors: systematic and random error [Fri12]. Systematic errors influence every measurement in a constant or predictable manner [Fri12] and can be divided into instrumental, environmental, observational and theoretical errors [Moh17]. Random errors vary in sign and weight and are caused by a change in experimental conditions, noise in the measuring instrument, voltage fluctuations during an experiment and other reasons [Fri12].

While systematic errors can be compensated to a certain degree, random errors can not be reduced [Fri12]. Although it is possible to reduce their impact on measurement results by

conducting several experiments series and calculating the average values [Moh17] [Fri12]. As a consequence, a newly developed measurement system must be evaluated regarding its suitability for the measurement task. Different performance characteristics for this evaluation suggested by the International Standard Organization (ISO) [DIN97] are depicted in figure 2.11.

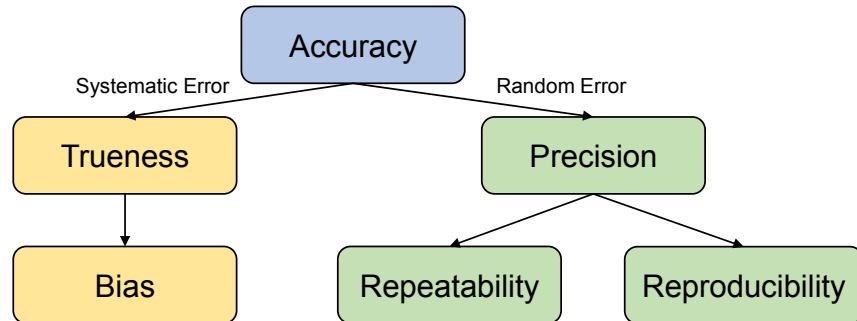


Figure 2.11.: Performance characteristics for measurement systems according to [DIN97].

According to the ISO, accuracy resembles the total error of a system and therefore is defined as the combination of both trueness and precision [DIN97] (figure 2.12). Trueness is defined as "the closeness of agreement between the arithmetic mean of a large number of test results and the true or accepted reference value" [DIN97, p. 9]. It is affected by systematic error and usually quantified through bias (total systematic error) [MPM07].

Whereas precision refers to "the closeness of agreement between independent test results obtained under stipulated conditions." [DIN97, p. 16] and is affected by random error and quantified through the standard deviation [MPM07]. Precision can be further divided into repeatability and reproducibility.

Repeatability is the variation between independent consecutive measurements of the input quantity obtained "with the same method on identical test items in the same laboratory by the same operator using the same equipment within short intervals of time." [DIN97, p. 17]. Whereas reproducibility is the variation between measurements of the same quantity obtained "with the same method on identical test items in different laboratories with different operators using different equipment" [DIN97, p. 17]. This thesis adheres to the definitions in [DIN97]. For a quantitative evaluation of these characteristics, a series of measurements can be conducted. Hereby the following metrics can be calculated.

A good estimate for the true value of a measurement is computed by taking the arithmetic mean \bar{x} of a series of measurements:

$$\bar{x} = \frac{1}{N} \sum_{i=1}^N x_i = \frac{x_1 + x_2 + \dots + x_N}{N} \quad (2.1)$$

where x_i is the measurement result of the i -th measurement of the quantity x and N is the number of measurements in the series [Din11]. This quantity is used for calculating the standard deviation s . It indicates the spread of individual measurements around the mean value:

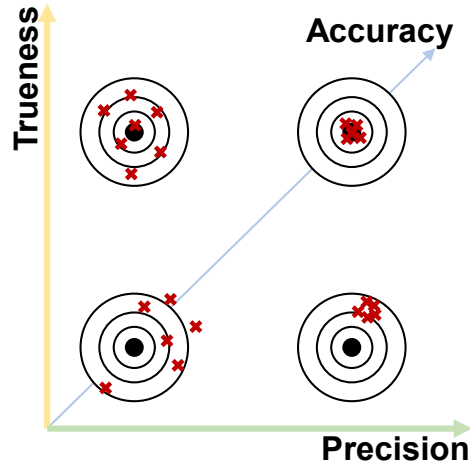


Figure 2.12.: Representation of the concept for accuracy, trueness and precision, as defined by [DIN97].

$$\begin{aligned}
 s &= \sqrt{\frac{1}{N-1} \sum_{i=1}^N (x_i - \bar{x})^2} \\
 &= \sqrt{\frac{1}{N-1} [(x_1 - \bar{x})^2 + (x_2 - \bar{x})^2 + \dots + (x_N - \bar{x})^2]}
 \end{aligned} \tag{2.2}$$

Provided an accepted reference value is available, the bias can be estimated by calculating the difference between the mean of a measurement series and the reference value [DIN97]. Calculating the standard deviation of a measurement series allows to quantify the repeatability and reproducibility depending on the experiment conditions [DIN97].

Now that the current state of research has been introduced, the concept and implementation of the experimental setup developed in the scope of this thesis is explained.

3. The Automated Test Setup

This chapter documents the process of developing the automated experimental setup. First, the system concept is explained. Secondly, the hardware integration and software implementation is presented.

3.1. Concept Development

The experimental setup developed in this thesis is intended for characterization and evaluation of tactile sensors for a robotic hand. The system concept is derived from the system requirements that are based on the specifications for tactile sensors in manipulation and the evaluation methods described in section 2.2.2. First, the requirements for the experimental setup are formulated. Then, the experiments designed for evaluating tactile sensors are explained. Finally, the system concept and the hardware components are introduced.

3.1.1. Setup Requirements

The following section describes the requirements for an experimental setup for the characterization and evaluation of tactile sensors for a robotic hand. These can be structured into requirements regarding experiment execution, force measuring capability and structure.

Experiments

As depicted in section 2.1.2, tactile sensors are required to detect normal and shear forces. Consequently, the experimental setup must be able to apply normal and shear forces.

The guidelines depict that forces between 0 and 10 N must be achievable.

Thereby the setup should be capable of controlling the applied normal and shear forces independently. This allows the calibration depicted in section 2.2.1 of the tactile sensor regarding normal and shear forces respectively. For shear forces the range of 0 N to 5 N is required to prevent damaging the sensors.

To determine the sensors sensitivity to small changes in pressure, the actuator should be able to apply forces with a high resolution. Therefore force steps of 0.01 N to 0.1 N should be attainable to test a sensitivity from 1g to 10g. For this, it is required to be able to vary the velocity at which the actuator moves towards the sensor surface.

According to section 2.1.2, the signal of a tactile sensor should be repeatable. Thereby the literature suggests no guideline for the minimum accepted repeatability of a tactile sensor. For evaluating this sensor characteristic, section 2.3.2 depicts that the environment conditions should be similar in between experiments. This includes the forces applied by the actuator.

To limit the variability of the reference data, the average force deviation between experiments

should not exceed 0.1 N. This requirement ensures that the reference data between repetitions of the same experiment does not vary more than the lowest force resolution that is required.

The setup must be able to execute the evaluation methods depicted in section 2.2.2 to determine the sensor characteristics depicted in section 2.1.2. For this, the actuator should be able to execute linear force loading with the above specified force requirements. Thereby, the linear loading should be executable in succession for the dynamic cyclic testing procedure. For the quasi-static method, the actuator must be capable of keeping a static force during dwell time. Additionally, it is required that the actuator is able to execute a sliding motion that tests the vibration sensing capabilities of a tactile sensor.

Shear force experiments must also be conductable independently and in combination with normal forces.

Thereby it is more desirable that the actuator is able to achieve the target forces within a threshold of 10% (1% for quasistatic) rather than keeping the average force deviation limit of 0.1 N between experiments. This to ensure that the actuator applies the depicted force curves for each procedure as intended. The procedures must be executable so that the sensor response to the specific curve is observable. The limit for the quasistatic testing is required to examine the sensor drift depicted in section 2.1.2 with a constant force.

Additionally, the actuator must be able to execute the testing procedures in an automated manner. This is to allow automated collection of reference data. Finally, the interface for the experiments should be user friendly to allow testing without requiring deep knowledge of the underlying control system.

Measurement

As highlighted in section 2.2.2, knowledge of the applied forces during experiments is required for sensor characterization and evaluation. For this, a force measuring instrument is needed. As normal and shear forces are applied during the experiments, the instrument needs to be capable of measuring 3D forces. Thereby forces between at least 0 - 10 N need to be measurable, as the experiments will be conducted with forces in the range of 0 - 10 N.

As stated in section 2.2.1, the accuracy of the reference data defines the possible calibration accuracy of a tactile sensor. Therefore an accuracy of 0.01 N to 0.1 N is required to be able to measure the smallest force the actuator is able to achieve.

Structural

Depending on the type of tactile sensor, a proper mount must be designed. Thereby the sensor should be in a fixed position to prevent any movement that distorts the measurements. Furthermore, the actuator movement should not be restricted by the sensor mount.

Additionally, the actuator probe should be interchangeable between different designs. This is required so that the tactile sensor can be subjected to different surface geometries as depicted in the literature by [YSP17] [Yua+15] [Tom+16].

Based on the requirements for tactile sensors the following experiments are designed. They depict the methods that are used to characterize and evaluate tactile sensors.

3.1.2. Experiment Design

The tactile sensors that will be evaluated first with this setup are embedded in a dome shaped silicone structure. For this reason, this tactile sensor structure is assumed in the experiments. This is indicated in figures 3.1 (a)-(d).

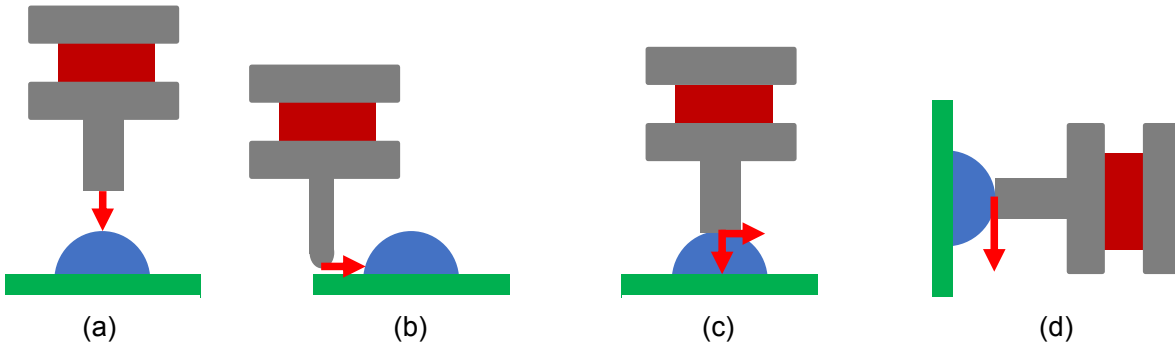


Figure 3.1.: Visualization for the planned experiments. (a) Linear, dynamic and quasistatic normal force. (b) Shear force to the side of the sensor. (c) Simultaneous normal and shear forces. (d) Sliding after establishing a contact force. A dome shaped sensor surface is assumed.

Normal Force. The requirements depict that the tactile sensor must be characterized regarding its ability to detect normal forces. The procedure for normal force characterization is shown in figure 3.1 (a). Thereby a sensor probe is driven perpendicular into the center of the upper side of the tactile sensor with a target force F_z of up to 10 N ($F_x, F_y = 0$). Here, a flat, rectangular probe is utilized. The size of the probe should be at least as large as the surface footprint of the tactile sensor to allow an even force distribution through out the sensor.

Thereby static and dynamic evaluation methods are executed. The graphs in figure 3.3 (a) depict the force curve that is applied for each method.

The linear force loading procedure is executed to measure the required reference data for the normal force calibration of the tactile sensor. The probe is lowered into the sensor surface and retracts with the same rate once the target force F_z is reached. As explained in section 2.2.2, this method also provides insight into sensor sensitivity, dynamic range, resolution and non-linearity.

The dynamic cyclic force procedure is conducted to collect data to determine signal repeatability, hysteresis, response time and dynamic signal drift of the tactile sensor. Thereby the procedure is conducted similarly to the linear normal force experiment, as depicted by the force graph in figure 3.3. Here, the linear forces are applied in succession with varying force rates.

The quasistatic cyclic procedure is conducted to collect data to determine signal stability, hysteresis and static signal drift. The graph in figure 3.3 shows how the force is applied for this procedure. The probe lowers into the sensor surface until a target force of F_z is measured. The probe then remains there for a dwell time of t_1 and retreats back from the surface once the time has passed. After a pause of t_2 this cycle is repeated.

Shear Force XY. This procedure is conducted to collect data for characterization and evaluation. The XY label indicates that only a shear force is applied. As depicted in figure 3.3

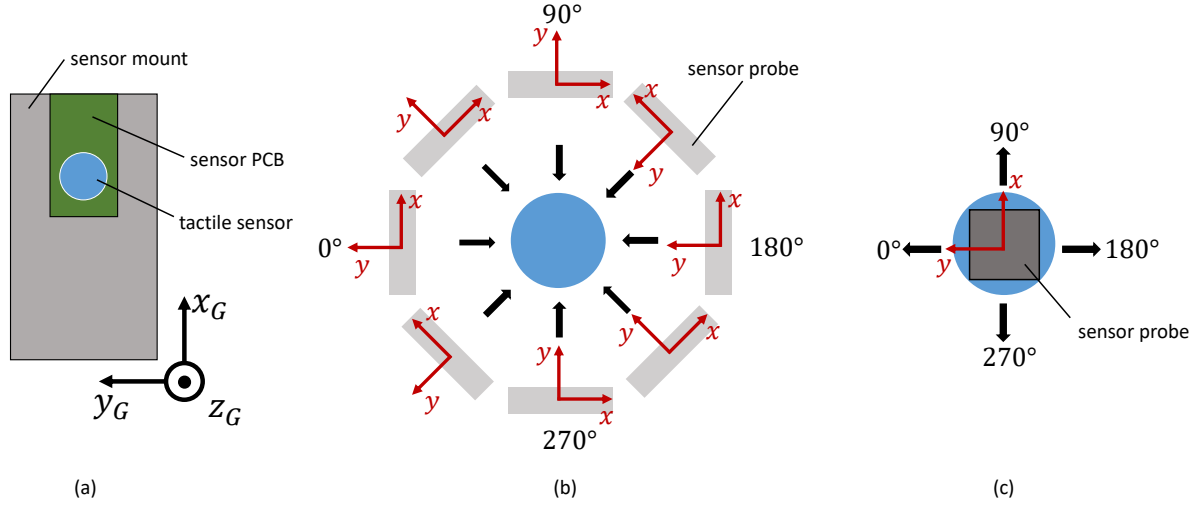


Figure 3.2.: Visualization for the shear force experiments. (a) Top view of the sensor mount. Indicated is the global robot coordinate system (b) Visualization for the XY shear force experiments. Indicated in red is the force sensor coordinate system. Movement direction of the probe is indicated by the black arrows (c) Visualization for the XYZ experiments.

(b), the probe is driven into the side of the sensor until a defined target force F_x, y ($F_z = 0$) is measured. The probe then retracts back to its initial position at the same force rate. This can be done in a 360° radius around the sensor center as shown in figure 3.2. Thereby, the sensor response to a shear force stimulus can be determined. The shear forces are limited to 5N to prevent damage on the sensor. A rectangular probe would not indent the surface evenly as the side is not flat but curved due to the dome shape. Therefore a circular probe is used to provide a more even distribution to the side.

Shear Force XYZ. This procedure is conducted to collect data for sensor characterization and evaluation. The XYZ label indicates that a normal force and shear force is applied. The force is applied as depicted in figure 3.3 (c). First the probe is driven perpendicular into the upper side of the sensor until a force target F_z is measured. Then, while F_z is kept constant, the probe is moved in either x or y direction to apply a target force F_x or F_y . Once this target is reached the probe releases the respective shear force. Finally, the probe releases the normal force. The shear forces are limited to 3N to prevent a sliding of the probe on the surface. Thereby this procedure is used to determine the influence of normal force on the shear force measurement of the tactile sensor. A flat, rectangular probe is used for the same reason as for the normal force experiments.

Sliding. This procedure is conducted to determine if a tactile sensor is capable of detecting vibration that indicates a sliding motion. As depicted in figure 3.1, the sensor is mounted in a vertical position. The probe is driven into the sensor surface until a contact force F_z (sensor coordinate system) is measured. Then, the probe slides down in negative z direction while keeping the contact force. Thereby a shear force F_y (sensor coordinate system) is measured induced from the sliding motion. This experiment is conducted with a flat probe to maximize the surface area in contact with the tactile sensor during the sliding motion.

The experiments explained above should all be executable with the experimental setup to allow characterization and evaluation. The following section describes the system concept and the different components.

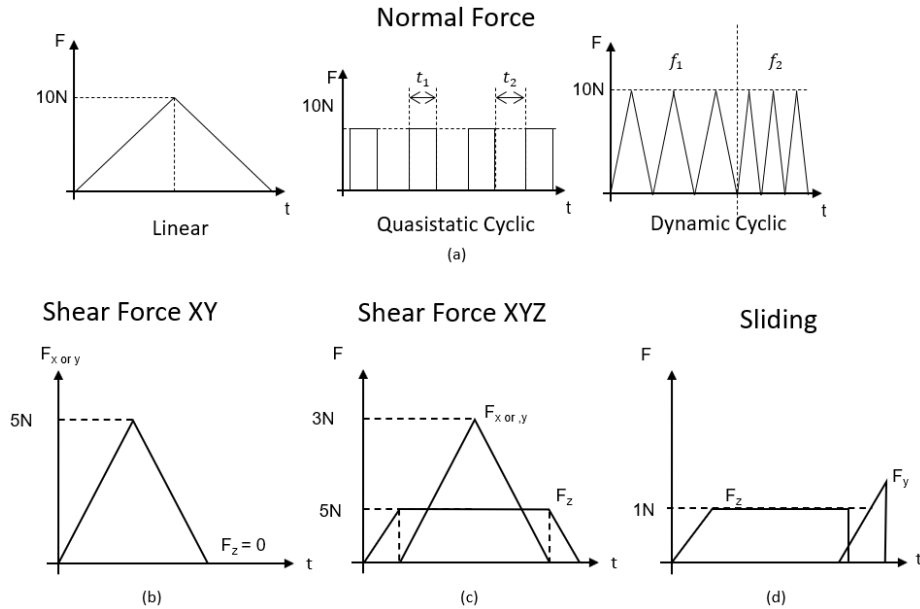


Figure 3.3.: The intended force curves for the experiments. (a) Linear, Quasistatic Cyclic and Dynamic Cyclic Normal Force. (b) Shear Force XY, (c) Shear Force XYZ, (d) Sliding.

3.1.3. System Concept

The system concept is based on the requirements depicted in section 3.1.1 and the experiments to be executed.

The general structure of experimental setups is outlined in section 2.3. Thereby the choice of actuator determines which test procedures are executable within the requirements. Table 3.4 shows an overview of the actuators with respect to how the procedures are conducted respectively.

As shown in section 2.3, it is possible to execute testing procedures without mechanical actuator. Thereby the forces can be applied either with weights or manual actuation. While using weights serves as a solution to provide reference data necessary for calibration, manual actuation delivers no information about the applied forces. Therefore no reference data is measurable for the procedures that are executed manually. As this violates the requirement that reference data is needed for every procedure, this solution is not viable.

As depicted in section 2.3, linear stages are utilized as actuators for experimental setups. They provide a high positional accuracy (0.01 mm [Yua+15], 100 nm [Lee+08], 0.5 μm [Wan+16]) and therefore the forces are applied with high precision. Thereby the linear stage is equipped with a probe and a force sensor to measure reference data. As shown in section 2.3 and depicted in the table 3.4, the linear stages require additional measures for the XY, XYZ and slip procedures.

		Actuator		
	Test Method	No mech. actuator	Linear Stage	Robot
Normal Force	Linear	Only Manual	1 Stag, probe displacement	Use End Effector
	Dynamic Cyclic	Only Manual	1 Stag, probe displacement	
	Quasistatic Cyclic	With Weight	1 Stag, probe displacement	
Shear Force	XY	With Weight	1 Stage with orientation platform req.	
	XYZ	With Weight	2-3 Stages needed	
Sliding		With Weight	1-2 Stages needed	

Figure 3.4.: Testing capabilities of actuators.

Thereby they need additional measures such as an variable orientation platform for the tactile sensors or multiple linear stages to enable movement in more than one direction.

Section 2.3 shows that the mobility of a robot arm is useful for testing tactile sensors. Thereby the end effector position is dynamically changeable and forces can be applied from various angles. Additionally, robot arms show high pose repeatabilities (± 0.03 mm for UR5e Robot [Rob21], ± 0.1 mm for Franka Emika Panda [Emi20]). With this, the robot is able to repeat a calibrated pose within the specified accuracy [DIN83]. For this reason, a robot arm is chosen as the actuator for this experimental setup. This enables the execution of the required procedures with a single actuator.

The robot chosen for this setup is a Panda Robot by Franka Emika [Emi20]. It provides internal force readings through joint torque measurements. Those have an accuracy of 0.8 N and a resolution of 0.05 N [Emi20]. To allow force sensing with an accuracy that meets the requirements, an external force sensor is needed.

For this, the K3D40 3-axis force sensor from ME-Meßsysteme [MM22b] is utilized. It is mounted at the end effector of the robot and measures the forces applied through a probe attached beneath it. This is depicted in figure 3.5. Also shown in the figure is a mounting structure for the tactile sensors. This is needed to prevent the sensors from shifting position when force is applied.

The final sensor calibration accuracy for the tactile sensors depends on two factors. This is depicted in figure 3.6. The accuracy of the force measurement has a direct influence on the calibration accuracy of the sensor. As explained in section 2.2.2, the reason for this is that the calibration can only be as accurate as the provided reference data.

The second factor originates from the actuation uncertainty of the robot. The commanded position forces can not be applied with perfect precision, which leads to varying forces between experiment repetitions. This does not have a direct impact on the measurement of the reference data, but rather on how much the reference data varies in between experiments. If the average of the reference data collected in a measurement series is calculated and used for calibration, this variability leads to a bigger standard deviation.

In the following the system components are introduced further.

The Robot Arm

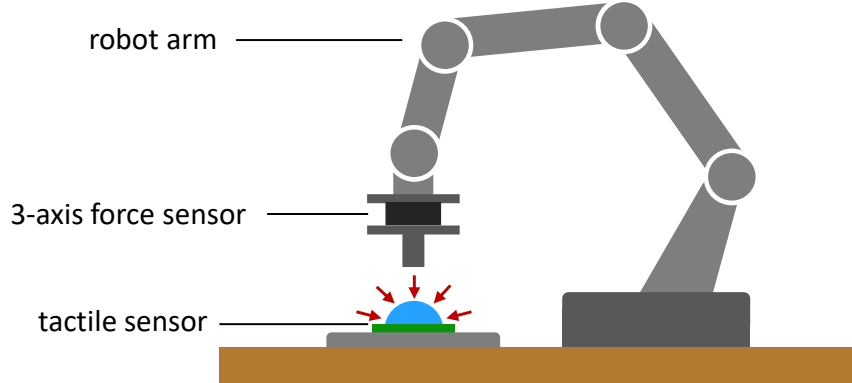


Figure 3.5.: Concept for the experimental setup. A robot arm is utilized to apply forces on tactile sensors. Thereby the forces are measured with a 3-axis force sensor.

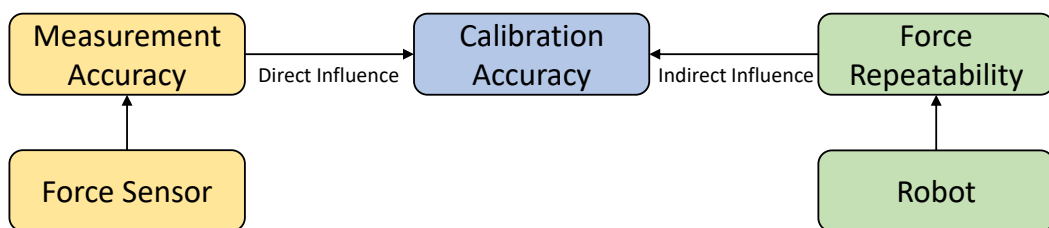


Figure 3.6.: Influences on the calibration accuracy of the tactile sensors. The measurement accuracy of the force sensor has a direct influence on the calibration accuracy of the sensor. The robots force repeatability has an indirect influence on the calibration accuracy.

The Panda Robot by Franka Emika [Emi22] is a 7 degree of freedom lightweight robot arm with a payload range of up to 3 kg (figure 3.7). Furthermore, it offers a certified (ISO 9283) pose repeatability of $< \pm 0.1$ mm with a path deviation of $< \pm 1.25$ mm and the end effector can reach up to 2 m/s [Emi20]. Thereby it has to be determined if the robot is able to apply the force during the procedures within the specified requirements (range, resolution, accuracy).

The robot can be controlled using the high-level, app-based "DESK" Interface or Franka Control Interface (FCI). The C++ library *libfranka* [Emi17] offers direct low-level control and access to internal measurements at 1 kHz by utilizing the FCI. *Libfranka* is integrated into several high-level, open-source libraries such as *franka_ros* or *Frankx* [Fra21] and *MATLAB Simulink*. Additionally, the motion control system *MIOS* is developed at MIRMI. It allows a realtime, task-based control of the robot.



Figure 3.7.: The Franka Emika Panda Robot [Emi20].

The Force Sensor



Figure 3.8.: (a) The K3D40 3-axis force sensor and the (b) GSV8-SD amplifier by ME-Meßsysteme [MM22b]

The K3D40 3-axis force sensor from ME-Meßsysteme [MM22b] is strain gauge-based sensor and measures up to 50 N. Its small size of 40 x 40 x 20 mm and light weight of 85 g is adequate for mounting on the Franka Emika Robot. Furthermore, it provides a base accuracy class of 0.5 %. For data collection, the sensor is connected to a GSV8-DS measurement amplifier from ME-Meßsysteme (figure 3.8(b)) that allows a readout frequency from 1 Hz to 48 kHz. The sensor data can be accessed through a USB-Port and an EtherCAT-Fieldbus on the GSV8-SD.

A high accuracy calibration of the sensor has been conducted by the manufacturer. Thereby the measurement system consists of the sensor and amplifier. In this process, the accuracy class is improved from 0.5% to 0.1-0.2% [MM22b]. The manufacturer (calibration certificate) states, that this results in 95% of the measurements lying inside a span of the specified class for the whole measurement range. For a range of 50N, this amounts to a force measurement of:

$$F_{meas} = F_{i,real} \pm e, e \in [0.05, 0.1]N \quad (3.1)$$

for every measured force F_x , F_y and F_z .

This range is within the required measurement accuracy depicted in the requirements.

To attach the K3D40 sensor to the robot arm, a corresponding mount is designed. Figure 3.9 shows the exploded (a) and unexploded (b) view of the end effector design. The two upper

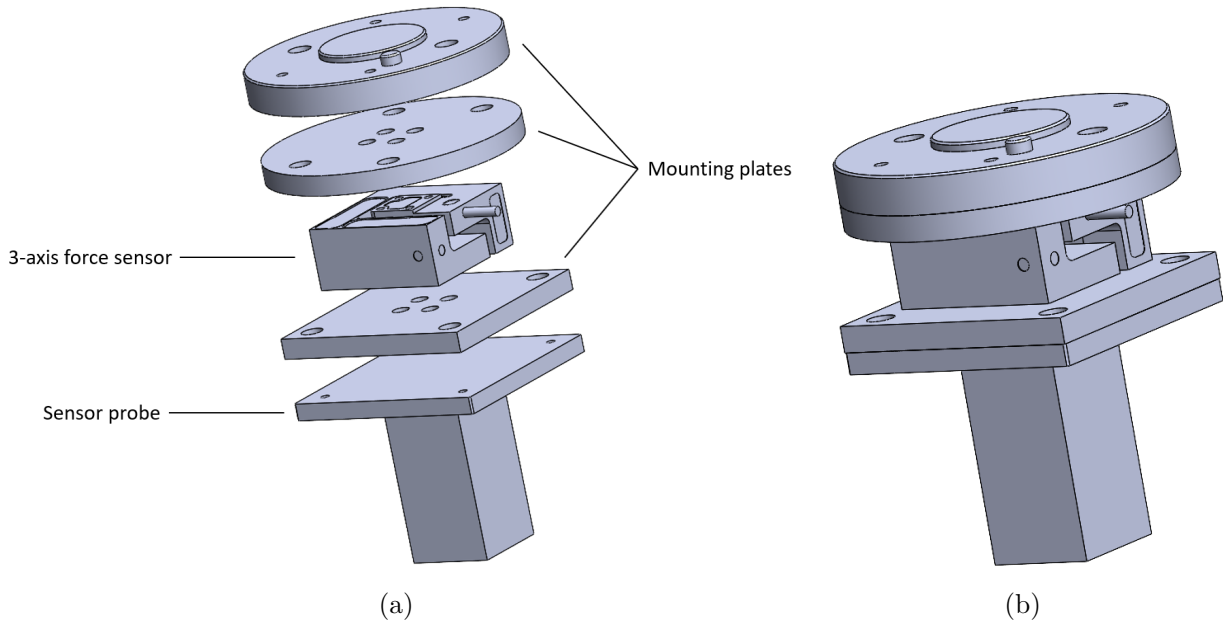


Figure 3.9.: The custom designed end effector. (a) Exploded View. (b) Normal View.

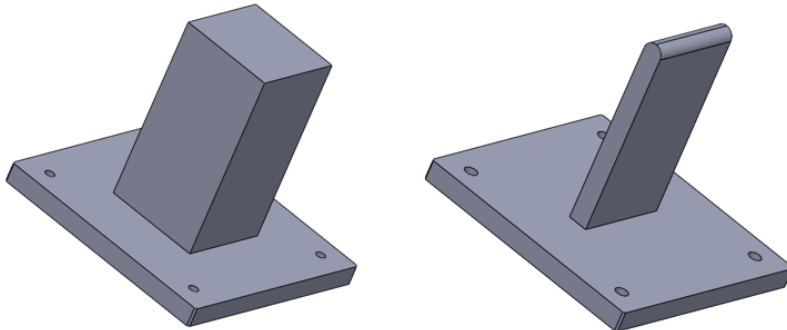


Figure 3.10.: Various sensor probes. (From left to right) A flat, circular ended and dope shaped probe.

mounting plates allow the sensor to be screwed to the robot end effector flange. A third mounting plate serves as base for the measuring probes. Thereby the probe is interchangeable so that different probe shapes are usable. Thereby figure 3.10 depicts the designs for the flat rectangular probe with a layout of 20x20 mm and a circular ended probe with a layout of 20x2.5mm.

The Tactile Sensor Mount

Different mounts are designed to enable fixating the tactile sensors. This is required to ensure that sensors do not shift position during experiments. The mount in figure 3.11(a) is used to secure the sensors in a horizontal position for normal and shear force experiments. For slip experiments, the mount in figure 3.11(b) is used. The vertical mount is initially designed so that the robot can execute a sliding motion by turning off gravity compensation. This should simulate an object sliding out of grasp. Both mounts provide a notch that can fit PCBs with a layout of 25x47x2 mm. These mounts are designed specifically for sensors that are in development at MIRMI. For sensors that have a different layout, additional mounts are required. Thereby the mounting structure must not obstruct the robot arm in its movement.

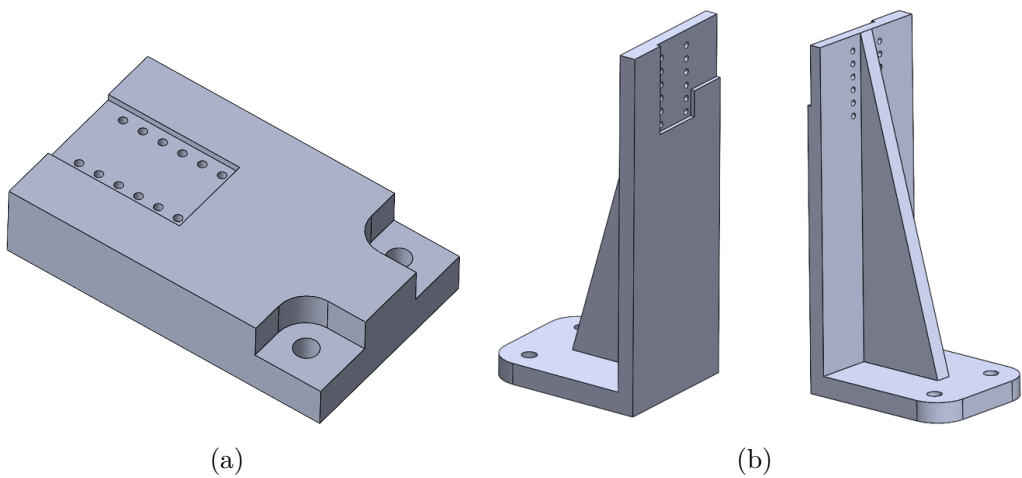


Figure 3.11.: The tactile sensor mounts. (a) horizontal and (b) vertical mounting structure.

3.2. Hardware Implementation

The following section explains the implementation process of the experimental setups.

Figure 3.12 depicts the assembled setup. It shows the robot arm mounted on a flat, sturdy table according to the user manual [Emi22]. Thereby it is ensured that the table is able to support the 17.8 kg of the robot and that it cannot collide with any objects in its working space.

The components for the force sensor mount are 3D printed with a Prusa i3MK3S 3D printer [Pru22] using Polyactid (PLA) material and a layer thickness of 0.2 mm.

The end effector is assembled according to figure 3.9(a). First, the two middle mounting plates highlighted are attached to the force sensor. Next, the remaining mounting plate is screwed to the robot flange. Finally, the sensor is mounted to the robot arm and the sensor probe is attached. Figure 3.12 shows the assembled end effector with the rectangular probe.

The tactile sensor mounts depicted in figure 3.11 are 3D printed with the Prusa i3MK3s printer using PLA and a layer thickness of 0.2 mm. The mounts are screwed to the table in front of the robot arm. Thereby it can reach the tactile sensors from any required direction. Figure 3.2 shows the horizontal sensor mount with a tactile sensor attached.

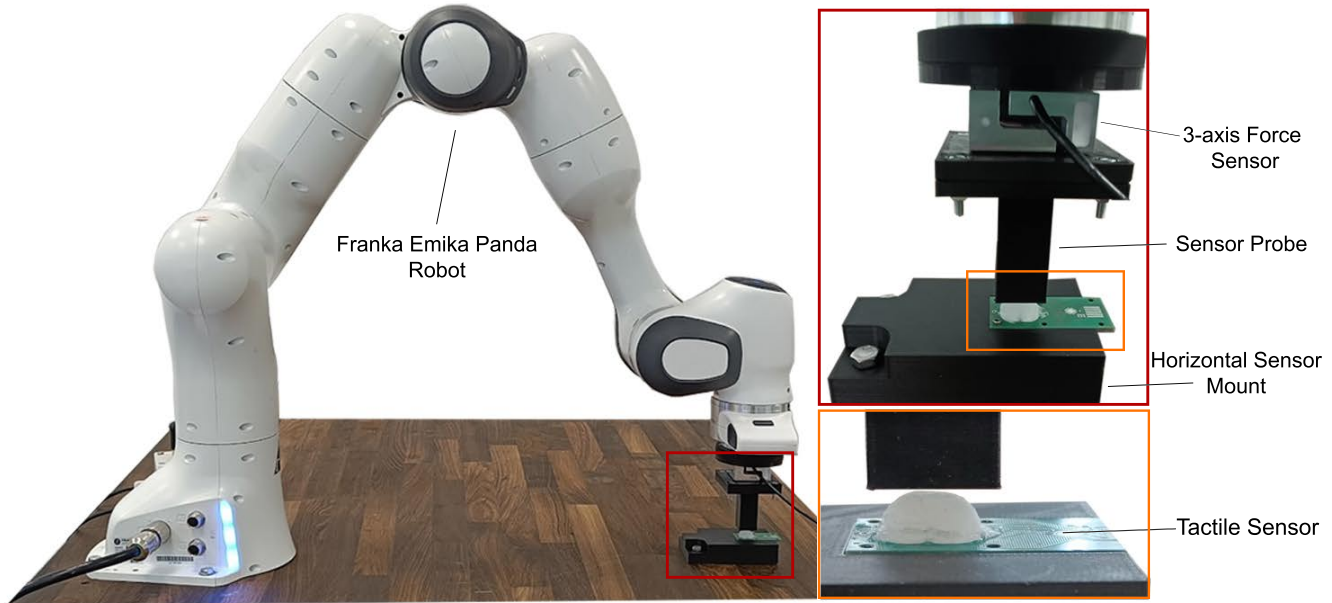


Figure 3.12.: The assembled experimental setup. Depicted is the Franka Emika Robot Arm that servers as actuator during experiments. A 3-axis force sensor is combined with custom designed end effector and attached to the robot to measure force reference data during experiments. A tactile sensor mount is designed and printed to fixate the tactile sensors.

3.3. Software Implementation

The following depicts the software implementation structure for the experimental setup. It is designed with regard to the requirements of user-friendliness and the capability for automation.

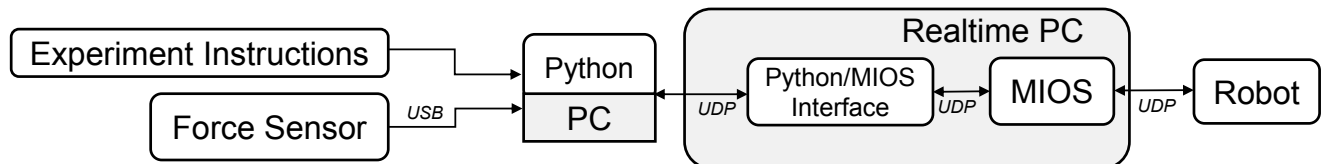


Figure 3.13.: Control concept of the system.

The control system consists of three different layers (see figure 3.13). At the lowest level is the MIOS motion control system, that offers a realtime, task-based control of the robot utilizing an impedance controller. Next is the Python-MIOS interface (PMi). It runs a state machine that receives input from Python, handles the transition between the steps of a procedure and executes the corresponding MIOS tasks accordingly. Thereby the end effector motion is executed by adapting the desired cartesian coordinates of the end effector and forwarding them to MIOS.

The Python layer servers two purposes: First, it reads the input data from the force sensor via a Universal Serial Bus (USB) connection and forwards it to the PMi using the User Datagram Protocol (UDP). This enables the interface to monitor the applied forces and react accordingly. Thereby it changes the desired coordinates based on the defined target forces.

Secondly, it sends the commands necessary for creating the experiment procedures to the

interface via UDP. The commands are defined in the interface. As an example, some viable commands can be found in table ???. They indicate which procedure the robot should execute and which parameters are desired.

Experiment procedures can be created by concatenating commands in a Python script. After sending a command to the PMi, the respective motion is executed and a response is received upon finishing the task. This signals that a new command can be sent.

As formulated in the requirements (section 3.1.1), this system enables the operator to generate different experiment sequences without requiring knowledge of the MIOS system. Additionally, the experiments are carried out with various parameters by changing the values in the commands. Furthermore, experiments can be repeated in succession for automated data collection. Thereby the robot returns to a starting point before each experiment run. This position is manually calibrated to make sure that the probe is centered above the sensor and the staring position is consistent.

A computer running a realtime kernel is required for the execution of MIOS. The PMi does not require a realtime kernel but is also executed the same machine. This machine is directly connected to the robot control unit via Ethernet. For the Python layer, a second PC is utilized that is connected to the network of the realtime PC and robot.

"Procedure" A "Parameter 1" B "Endmotion"	Execute procedure with target force A and value B for parameter 1 and execute the specified endmotion
F 5 R 0.0001 Back	Apply force normal to the sensor, with a velocity of $0.0001 \cdot 250 = 0.025 \frac{m}{s}$ until 5 N are measured, then retreat back to initial position

Table 3.1.: Example command for the experiment procedures. The calculation for velocity originates from the implementation in the PMi.

4. Evaluation

While the preceding chapter concerns itself with the concept development and implementation of the experimental setup, the following chapter focuses on its evaluation.

As explained in section 3.1, the experimental setup can be examined from two angles: First, its ability to accurately measure the applied forces may be evaluated. The force readings are influenced by the accuracy of the utilized force sensor and the force transmission through it. Using a probe to apply the forces induces a bias in the force sensor. This is depicted in figure 4.1.

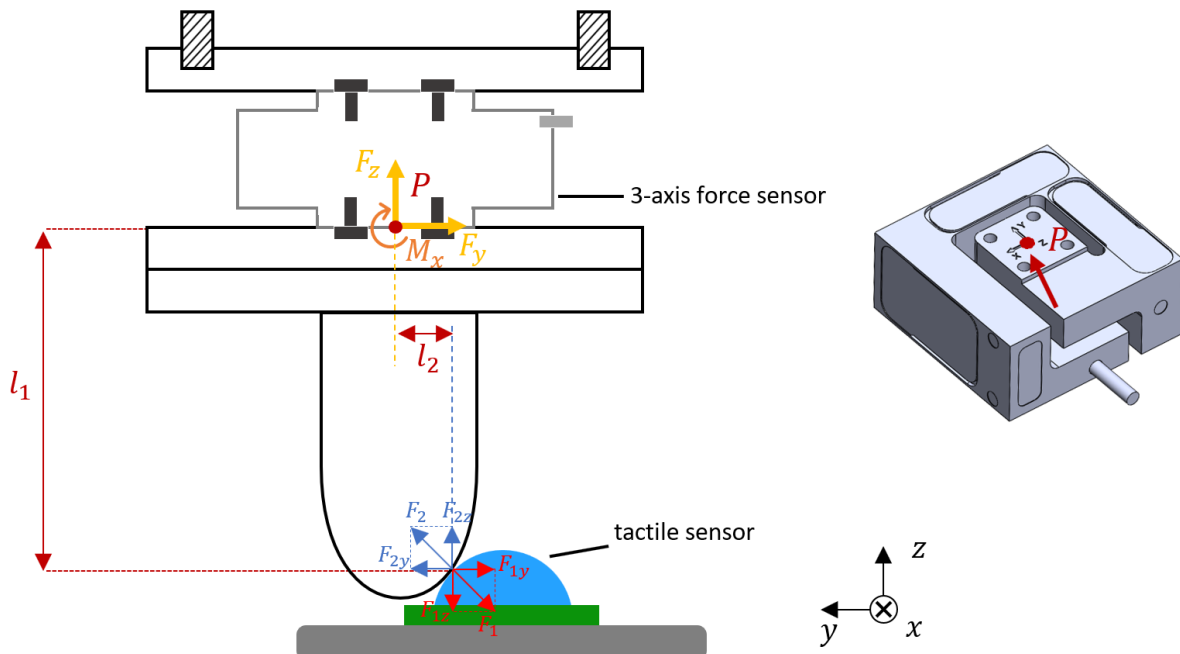


Figure 4.1.: Visualization of the sensor mounting and sensor probe on the force measurements.

Due to the depicted coordinate system on the sensor (right side) and the lack of documentation from the manufacturer regarding the internal functions, the pivot point P is assumed as indicated in the figure.

As the probe moves into the side of the sensor, the forces F_2 and F_1 occur. Thereby these forces can be decomposed in their respective y and z components. Due to the displacement l_1 and l_2 this results in a torque M_x around P . Thereby the following equations are derived:

$$\begin{aligned} -F_y + F_{z,y} &= 0 \\ F_z + F_{2,z} &= 0 \\ M_x - F_{2,z} \cdot l_2 + F_{2,y} \cdot l_1 &= 0 \end{aligned} \quad (4.1)$$

these can be changed into:

$$\begin{aligned} F_y &= +F_{2,y} \\ F_z &= -F_{2,z} \\ M_x &= F_{2,z} \cdot l_2 - F_{2,y} \cdot l_1 \end{aligned} \quad (4.2)$$

We know the maximum values for $l_1 = 59mm$ and $l_2 = 2.5mm$ from the size of the measurement probe and thickness of the mounting plates.

The sensor shows a crosstalk value of for $1\% \cdot \frac{50N}{2Nm}$ from x/y to z [MM22a]

Assuming forces of 5N for F_z and F_y , we can calculate that $M_x = 5N \cdot 0.0025m - 5N \cdot 0.059m = -0.2825Nm$

Using the crosstalk uncertainty we get that $|\frac{0.5N}{2Nm} \cdot -0.2825Nm| = 0.070N$

This error has to be considered when sensor calibration is executed.

As this is a worst case estimation for a shear force of 5N, this error is not considered in the subsequent evaluation.

Secondly, the experimental setup can be analyzed regarding its capability to reliably apply forces and carry out the planned procedures depicted in section 3.1. Thereby it must be ensured that every experiment procedure can be executed as intended and thereby produce consistent results. As explained in section 3.1, the actuator is not able to perfectly execute the forces. Therefore it has to be determined if the capabilities of the robot are within the requirements. For this, experiments are conducted.

4.1. Results

The conducted experiments coincide with the planned experiments in 3.1. This is done to examine if the setup meets the formulated requirements necessary for characterizing and evaluating tactile sensors. The tests are executed on a tactile sensor dummy depicted in figure 4.2. It consists of a dome shaped silicone mould glued to a printed circuit board (PCB) (figure 4.2) and is modelled after the real sensors that will be tested with the experimental setup.

The following presents the results of the experiments for linear, cyclic and quasistatic normal force as well as shear XY / XYZ and sliding.

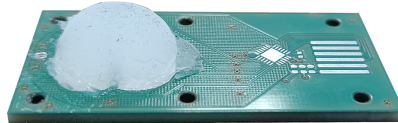


Figure 4.2.: The tactile sensor dummy. A dome shaped silicon mold glued to a PCB.

Linear Normal Force

The results of the linear normal force experiments are depicted in figure 4.3. Thereby figures (a,b), (c,d) and (e,f) show the same experiment. The figures (a), (c), (e) depict the averages forces F_x , F_y and F_z and their standard deviations that are measured over 25 (a), 25 (c), 5 (e) experiment repetitions. The figures (b), (d), (f) depict the average force F_z and the relative probe movement in z-direction. Thereby the position at the point of contact with the sensor serves as reference point regarding the relative movement.

Each experiment has the same force target of $F_z = 10.00$ N, $F_x, F_y = 0$ N. The probe has a target velocity of 25 mm/s, 0.25 mm/s and 0.025 mm/s for (a), (b) and (c) respectively. Thereby a maximum normal force $F_{z_{max}}$ (blue line) of 11.39 N, 9.99 N and 10.08 N is reached for (a), (b) and (c). This results in average force rates of 39.29 N/s, 0.33 N/s and 0.03 N/s. The standard deviations for the loading phase are 0.28 N, 0.11 N, 0.03 N and for de-loading 0.34 N, 0.21 N, 0.02 N respectively for (a), (b) and (c). The normal forces are expected.

Thereby the experiments exceed their respective force target of $F_z = 10$ N (a),(b),(c) by 13,9% (a), 0.1 % (b) and 0.8 % (c).

Each experiment displays shear forces in x and y direction. The highest shear forces are ($F_{x_{max}} = -0.61$ N (green line), $F_{y_{max}} = -0.39$ N (red line)) in (a). For (b) and (c) shear forces are measured with $F_{x_{max}} = -0.37$ N, -0.36 N and $F_y = -0.26$ N, -0.37 N. These shear forces are not expected in this experiment.

Depicted in the figures (b), (d), (f) are the lines l_1 (green), l_2 (black) and l_3 (yellow). Thereby l_3 , l_1 show the slope of the average probe velocity loading/unloading phase. l_2 marks the point in time where the maximum probe displacement is reached. The average velocities for loading/unloading are 9.35 mm/s, 5.57 mm/s (a,b), 0.09 mm/s, 0.08 mm/s (c,d) and 0.009 mm/s / 0.008 mm/s (e,f). Thereby the maximum relative replacement reaches $z_{relmax} = 2.62$ mm (a,b), 2.88 mm (c,d) and 2.97 mm. Here, a deviation of the probe velocity regarding the target speed is expected but not to this extend. Thereby the measured velocities reach 37.4% / 22.28% (a), 36% / 32% (b) and 36% / 32% (c) of the target speed. It is not intended that the probe speed varies.

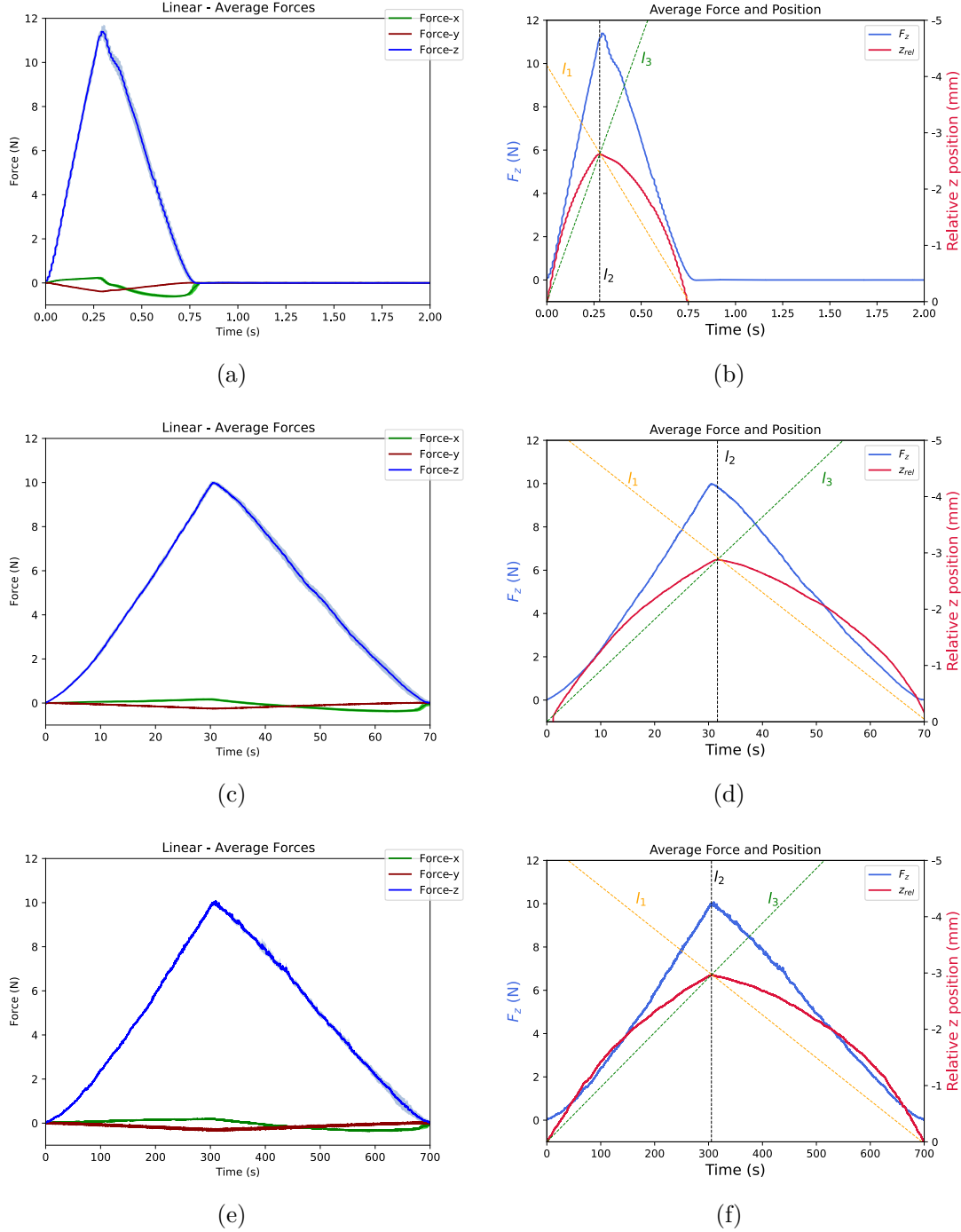


Figure 4.3.: Experiments for evaluation of linear normal force procedures. Target force of $F_z = 10\text{N}$, $F_x, F_y = 0\text{N}$ for every experiment pair (a,b), (c,d), (e,f) . End effector target velocities of 25 mm/s (a),(b), 0.25 mm/s (c),(d) and 0.025 mm/s (c).

Dynamic Normal Force

The figure 4.4 displays the results of the dynamic normal force experiments. The figures (a), (b), (c) and (d) depict the averages forces F_x , F_y and F_z and their standard deviations that are measured over 15 (a), 25 (b), 25 (c) and 25 (d) experiment repetitions. The force targets for the experiments are $F_x, F_y = 0 \text{ N}$ (a-d) and $F_z = 1 \text{ N}$ (a), 1 N (b), 10 N (c) and 10 N (d). Target

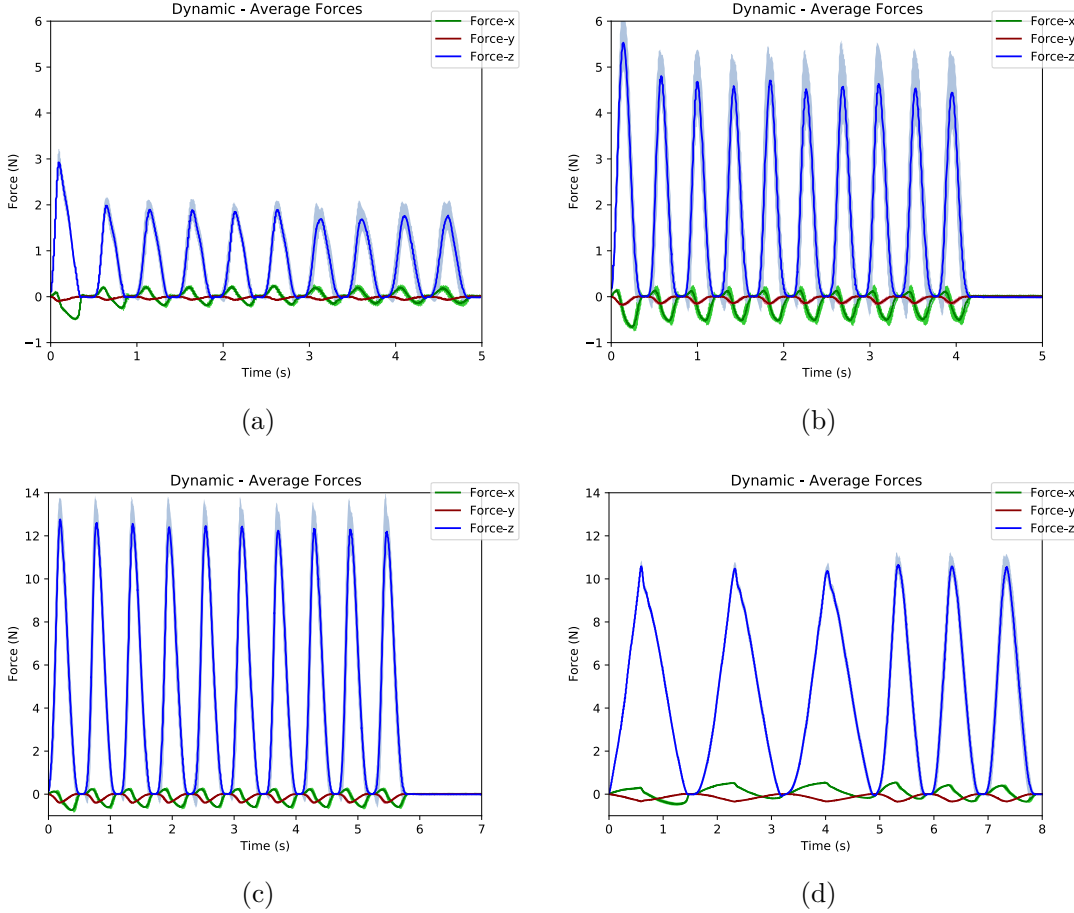


Figure 4.4.: Experiments for evaluation of dynamic normal force procedures. Target force of 1 N for (a),(b); 10 N for (c),(d). Probe target velocities: 25 mm/s (a), 50 mm/s (b), 50 mm/s (c), 12.5 & 25 mm/s (d)., 15 (a), 25 (b), 25 (c) and 25 (d) experiment repetitions.

probe velocities are 25 mm/s (a), 50 mm/s (b), 50 mm/s (c), 25 (cycle 1-3) & 50 mm/s (cycle 4-6) (d) respectively.

In **(a)** the normal force is applied for 10 cycles. The initial peak for F_z is at 2.92 N while the following repetitions show lower peaks at 1.92 N (repetition 2-6) and 1.76 N (rep. 7-10). The average standard deviation (SD) for F_z is 0.19 N (rep. 1-6) and increases to 0.30 N for rep 7-10.

Similarly, in **(b)** the normal force is applied for 10 cycles. Thereby higher peaks of $F_z = 5.93$ N (rep. 1) and 4.44 N to 4.81 N (reps. 2-10) are observed. The average standard deviation for F_z at the peaks is 0.97 (rep. 1-6) and increases to 1.12 N (rep. 7-10).

For the experiment depicted in **(c)** the normal force is applied for 10 cycles. The average peak height is at $F_z = 12.45$ N. The average standard deviation for the peaks increases from 1.29 N to 1.72 N.

The experiment conducted in **(d)** shows that peaks for F_z are 10.64 N on average. The standard deviation for F_z at the peaks is 0.24 N (rep. 1-3) and 0.81 N (rep. 4-6).

Thereby the experiments exceed their respective force target of $F_z = 1\text{N}$ (a),(b) & 10N (c),(d) by 192% (rep. 1) & 92% (rep. 2-6) & 76% (rep. 7-10) (a), 493 % (rep. 1), 381% (rep. 2-10) (b),

24.5 % (c) and 6.4 % (d).

Similar to the linear force experiments, shear forces are measured during loading and deloading phases. Thereby the average shear forces are $F_x = 0.21$ N (a), -0.59 N (b), -0.61 N (c), 0.42 N (d) and $F_y = -0.9$ N (a), -0.13 N (b), -0.34 (c) and -0.26 (d).

The average velocities for loading/unloading are 11.98 mm/s , 8.14 mm/s (a) , 19.77 mm/s , 13.18 mm/s (b) and 21.60 mm/s / 11.78 mm/s (c) and 4.54 mm/s / 3.09 mm/s (rep. 1-3) & 8.91 mm/s and 5.21 mm/s (rep. 4-6) (d).

Thereby the measured velocities reach 47.92% , 32.56% (a), 39.54%, 26.36% (b), 43.2% , 23.56% (c) and 36.32% , 24.72% & 35.64% , 20.84 % (d) of the target speed.

Quasi-Static Normal Force

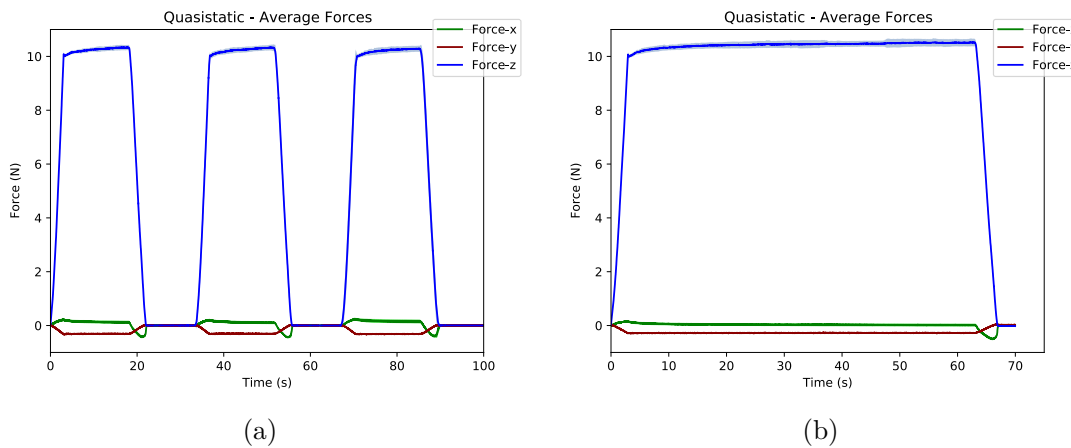


Figure 4.5.: Experiments for evaluation of quasi-static normal force procedures. Target force of 10 N for both experiments. Dwell time of 15s (a) and 60s (b). 15 repetitions for (a) and (b)

The results of the quasi-static force experiments are depicted in figure 4.5. The figures (a) and (b) depict the averages forces F_x , F_y and F_z and their standard deviations that are measured over 15 (a) & (b) experiment repetitions.

The experiment conducted in (a) has a target force of $F_z = 10$ N & $F_x, F_y = 0$ N for a total of 3 loading cycles. Each peak has a dwell time of 15s. A force drift of 0.47 N, 0.26 N and 0.25 N can be observed for every cycle respectively. The cycles are separated by a pause of 10s.

The experiment in figure (b) consists of a single quasi-static cycle with a dwell time of 60 s and a target force of $F_z = 10$ N. The force drift is measured to be 0.51 N.

Thereby it is expected that the force remains static and no drift occurs.

Thereby the experiments exceed their respective force target of $F_z = 10$ N (a),(b) by 4.7%, 2.6%, 2.5% (a), 5.1 % (b). Thereby the force F_z shows an average deviation of 0.17 N (a) and 0.25 N (b).

Again, shear forces are observed during each cycle. F_y and F_x are on average 5.1 % of the force target for F_z .

Shear Force XYZ

The results of the XYZ shear force experiments are shown in figure 4.7. Every experiment is repeated 15 times has a tangential target force of 3N with an initial normal force of $F_z = 5\text{ N}$ applied. The probe has a target velocity of 2.5 mm/s. Thereby the shear force is directed as depicted in figure 3.2 (c). The experiments are conducted by steps of 45° to examine the actuator behaviour for movements in positive/negative x/y as well as combined directions.

The figures (a) (0°) and (b) (180°) both show an initial normal force loading to $F_z = 5.11\text{ N}$ and 5.08 N . Whereas in (a), the normal force F_z has a slight increase/decrease of 0.33 N during tangential loading/delowering, the normal force in (b) decreases/increases by 0.39 N. A maximum force of $F_y = -2.97\text{ N}$ and 2.98 N is measured for (a) and (b) respectively.

The experiments in (c) (45°), (e) (90°) and (g) (135°) show the initial force load F_z of approx. 5N. This is intended as a constant normal force during the lateral loading is planned. The force F_z remains at this magnitude for the duration of the lateral loading phase, this is indicated by the increasing shear forces F_x (green line) and F_y (red line). Once the lateral delowering is started (indicated by the decreasing shear forces), the normal force increases to to $F_{z_{max}} = 8.94\text{ N}$ (c), 9.48 N (e) and 8.77 N (g). Thereby the normal force (blue line) deloads back to $F_z = 0$ once the lateral shear force is unloaded.

This behaviour is mirrored for the experiments in (d) (225°), (f) (270°), (h) (315°). The initial normal force does not reach a constant level at the target force $F_z = 5\text{ N}$ as it does for (c), (e) and (g). Instead it increases directly to $F_{z_{max}} = 7.98\text{ N}$ (d), 8.32 N (f), 8.49 N (h). At that level F_z reaches a static phase for approx. 1s until the shear force is deloaded (indicated by the green and red line decreasing).

The maximum average shear force is $|F_{xy_{max,avg}}| = 2.98\text{ N}$. This results in a deviation of 0.6% regarding the target force. For the experiments (c), (d), (g), (h) with both F_x and F_y component, the total shear force is given through the addition of both vectors.

For each experiment, the force F_z is expected to behave similarly to that in (a). Exceeding the target force of $F_z = 5\text{ N}$ is not intended. Thereby the target force is exceeded by 2.2% (a), 1.6% (b), 78,8% (c), 59,6% (d), 89,9% (e), 66,4% (f), 75,4% (g) and 69,8% (h) respectively.

It is not expected that the actuator behaviour varies based on which direction ($\pm x/y$) the force is pointed to.

Shear Force XY-Plane

The results of the XY shear force experiments are shown in figure 4.7. The figures (a) and (b) depict the averages forces F_x , F_y and F_z and their standard deviations that are measured over 15 (a), 15 (b) experiment repetitions. Every experiment has a target force of $F_y = 5\text{ N}$ & F_x , $F_z = 0\text{ N}$ and a target probe speed of 2.5 mm/s.

As depicted in figure 3.2 (b), the probes starting position around the sensor increases from 0° to 315° with steps of 45° for every experiment. Thereby the actuator behaviour for movements in positive/negative x/y as well as combined directions is observed.

Due to limits in the last robot joint, the force sensors axis rotates around 180° for the experiments from 135° to 270°. This is depicted in [3.2](#). Thereby the positive y-axis is pointing towards the movement direction of the probe. This results in a negative force being detected once the tactile sensor pushes back into the probe. This explains the change of sign for F_y in (g) and (h).

For **(a)** (0°) and **(b)** (180°), a force of $F_y = 4.91$ N, -5.02 N and $F_z = 3.1$ N, 3.15 N is reached. Thereby the average deviations are 0.06 N (a), 0.06 N (b) for F_y and 0.04 N (a), 0.04 N (b) for F_z .

For the experiments **(c)** (45°), **(e)** (90°) and **(g)** (135°) an average initial force F_z up to 1.92 N is observed. The F_z force reaches 3.40 N (SD = 0.19 N), 3.06 N (SD = 0.27 N) and 2.93 N (SD = 0.18N) respectively for **(c)**, **(e)**, **(g)** during the lateral loading. Thereby each experiment shows a maximum force F_y of 4.86 N (SD = 0.23N), 4.68 N (SD = 0.37 N) and -4.82 N (0.27 N). The experiments **(d)** (225°), **(f)** (270°), **(h)** (315°) show the average maximum forces F_z of 4.48 N (SD = 0.13 N), 5.47 N (SD = 0.15 N) and 5.44 N (SD = 0.13) and F_y of -5.01 N (SD = 0.08 N), -5.00 N (SD = 0.10 N) and 4.98 N (SD = 0.11). Thereby the normal forces F_z reach a similar magnitude as the forces for F_y . The normal forces are not expected.

The average maximum shear force is $|F_{y_{max,avg}}| = 4.92$ N. This results in a deviation of 1.6% regarding the target force.

Sliding

The results of the sliding experiments are shown in figure [4.8](#). Both experiments in **(a)** and **(b)** are repeated 20 times and have a target normal force of $F_z = 1$ N and a target sliding velocity of 2.5 mm/s and 25 mm/s respectively.

An average contact force of $F_z = 1.26$ N (SD = 0.14 N) **(a)** and 1.18 N (SD = 0.15 N) **(b)** is observed. Thereby the target force $F_z = 1$ N is exceeded by 26% (a) and 18% (b). The contact force is held for two seconds before sliding.

In **(a)**, the normal force F_z increases to 3.08 N (SD = 0.26 N) during the sliding motion. At the same time, shear forces of $F_x = 0.54$ N (SD = 0.07 N) and $F_y = -2.99$ N (SD = 0.20 N) can be observed. This is similar for **(b)** where the forces rapidly change to $F_x = 0.57$ N (SD = 0.12 N), $F_y = -2.66$ N (SD = 0.53 N) and $F_z = 2.42$ N (SD = 0.50 N).

Whereas the shear force F_y during sliding is intended, the forces F_z and F_x are unexpected.

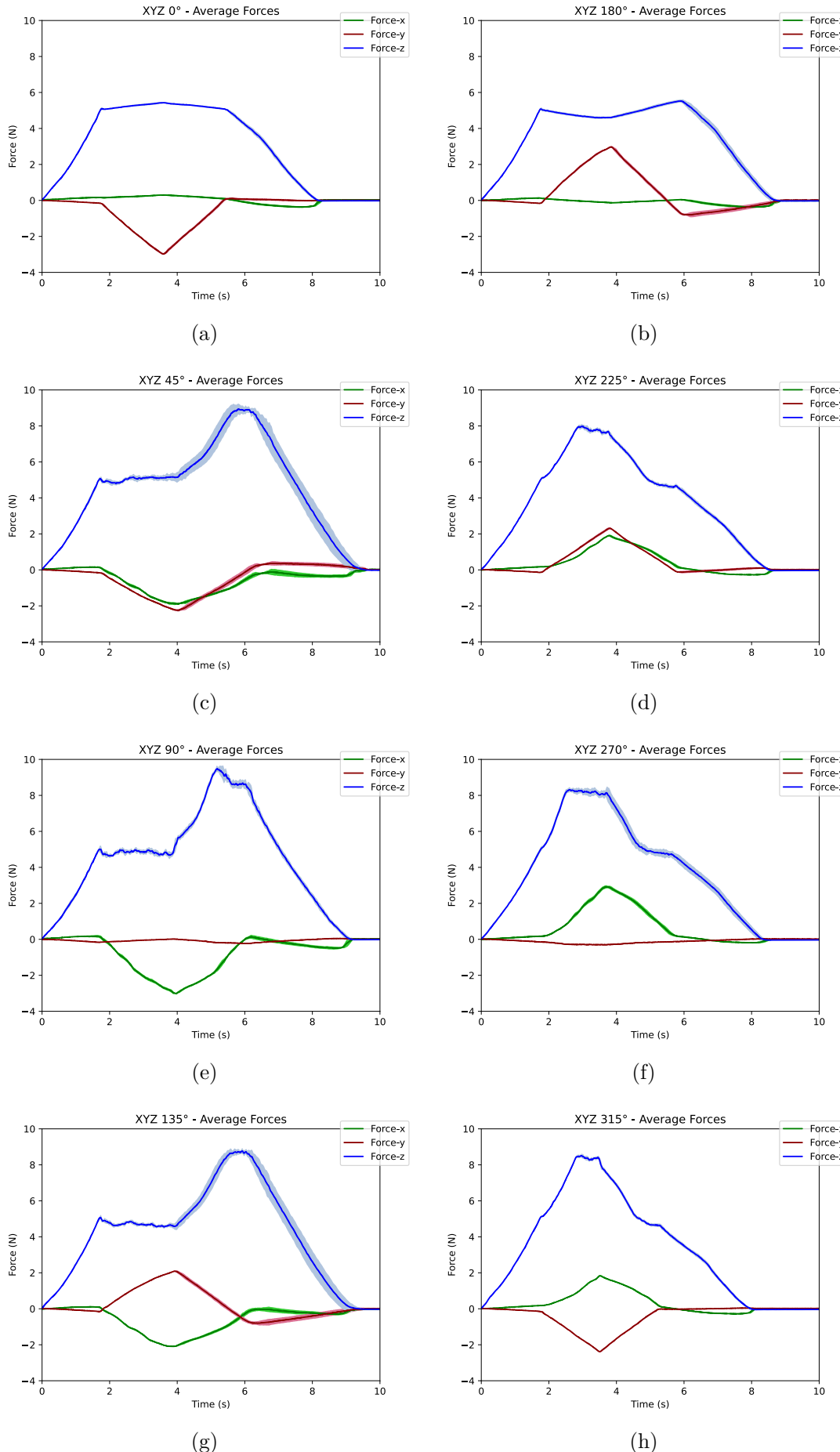


Figure 4.6.: Experiments for feasibility of shear force XYZ procedures. Initial normal force of 5N. Target shear force of 3N for every experiment. Varying angles from 0° to 315° in 45° steps. Target Probe velocity of 2.5 mm/s. 15 Repetitions each.

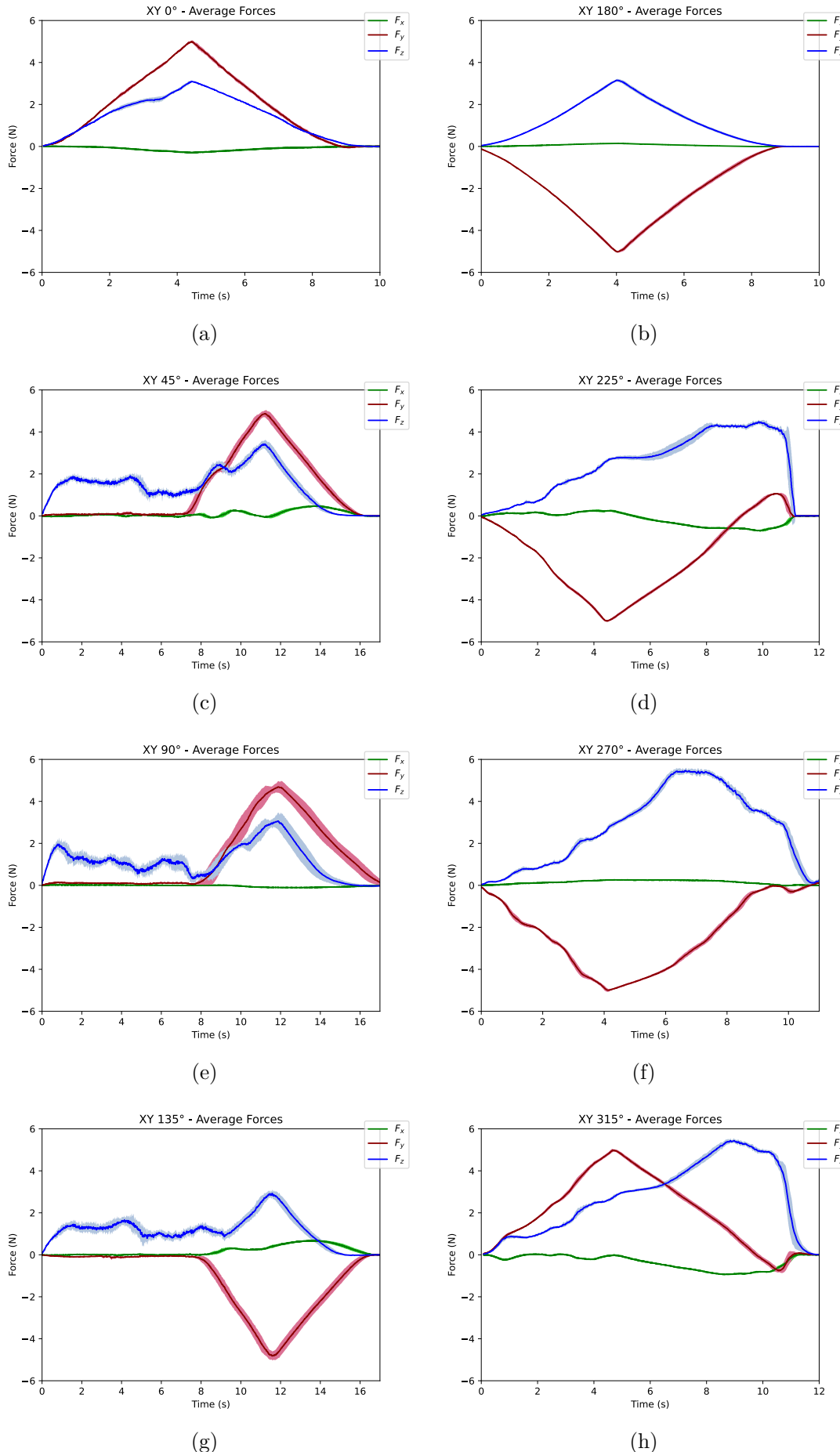


Figure 4.7.: Experiments for evaluation of shear force XY procedures. Target shear force of 3N for every experiment. Varying angles from 0° to 315° in 45° steps. Probe velocity of 2.5 mm/s. 15 Repetitions each.

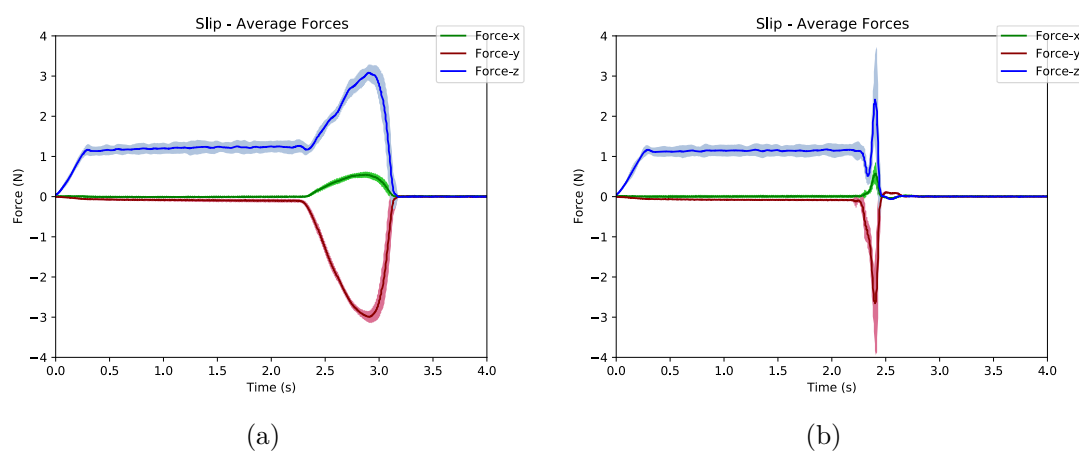


Figure 4.8.: Experiments for evaluation of sliding procedures. Target contact force of 1N. Probe velocity of 2.5 mm/s (a) and 25 mm/s (b). 20 repetitions each.

4.2. Discussion

The succeeding discussion aims to evaluate the experimental results. Thereby the results are examined regarding the formulated requirements for the experimental setup. Additionally, the unexpected behaviour is explained.

Linear Normal Force Experiments

Requirements. The linear loading experiments demonstrate the setups capability to apply normal forces onto the tactile sensor surface. The results depict that normal forces between 0-10 N are achievable. Thereby a minimal force resolution of 0.03 N/s can be applied. This is within the formulated requirement for the force range and minimal force resolution. In these experiments, the actuator exceeds the target force between 0.1 % to 13.9 %. This value varies based on the probe velocity in z-direction in the loading phase. Considering the measured probe velocities (z-direction) in the linear and dynamic cyclic experiments (during loading), the relationship shown in figure 4.9 is determined.

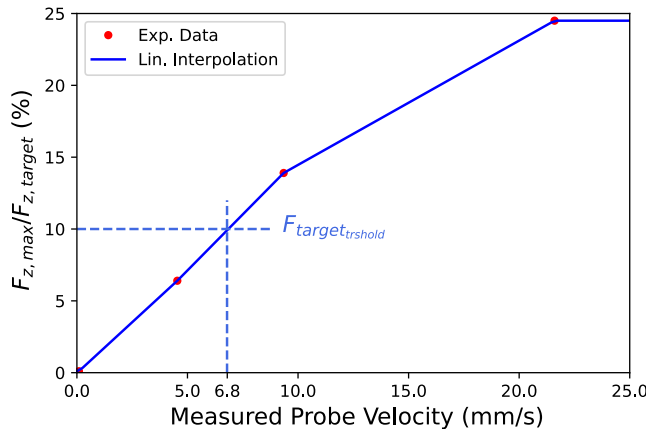


Figure 4.9.: The relation between exceeded target force and probe velocity in z-direction.

Thereby the blue line depicts the value of $F_{z,max}/F_{z,target}$ for a target force of $F_z = 10\text{N}$ with regard to the measured probe velocities of the respective experiment. This relationship indicates that the probe velocity in z-direction should not exceed 6.8 mm/s so that the normal force F_z stays within the formulated maximum target force deviation of 10% for the operating range of 10N. For these experiments, the normal force is applied as expected. However, they show an average deviation of up to 0.28 N and are therefore not within the specified limit of 0.1N for the average force deviation between experiments.

Additionally, the results show that shear forces are measured during experiments. This means that the forces F_x , F_y are not entirely controllable during this procedure.

Analysis. The shear forces F_y and F_x for the linear experiments are assumed to have several possible origins. First, it is considered that the end effector is not able to execute a perfectly vertical movement. The relative probe displacement and averages forces during the linear experiment depicted in 4.3(b) are shown in figure 4.10. The probe position is considered relative to the point of contact where the probe first touches the sensor surface. During the loading phase the displacement in x direction non zero value shows no significant movement. However,

once the deloading phase begins (starting point indicated by the vertical line) the probe shows a movement of $x_{rel} = 1.8$ mm until the end of the experiment. Thereby the shear forces depicted in the upper figure of 4.10 are measured by the force sensor. Due to the robots possible path deviation of up to ± 1.25 mm a strict vertical movement can not be guaranteed. Utilizing a guiding rail that limits lateral movement during the experiment is assumed to be a possible solution to this.

The shear forces observed in the subsequent dynamic and quasi-static experiments have the same origin.

Additionally it must be noted that the target velocity for the probe movement does not correspond with the actual measured velocities. A possible origin for this is the physical resistance of the tactile sensor. This can be seen in figure 4.10. Thereby z_{rel} shows the nonlinear movement of the probe resulting from the resistance through the silicone material.

The reduced probe velocity that is depicted in the figure is possibly a result of the gravity acting on the robot arm and therefore slowing down the movement.

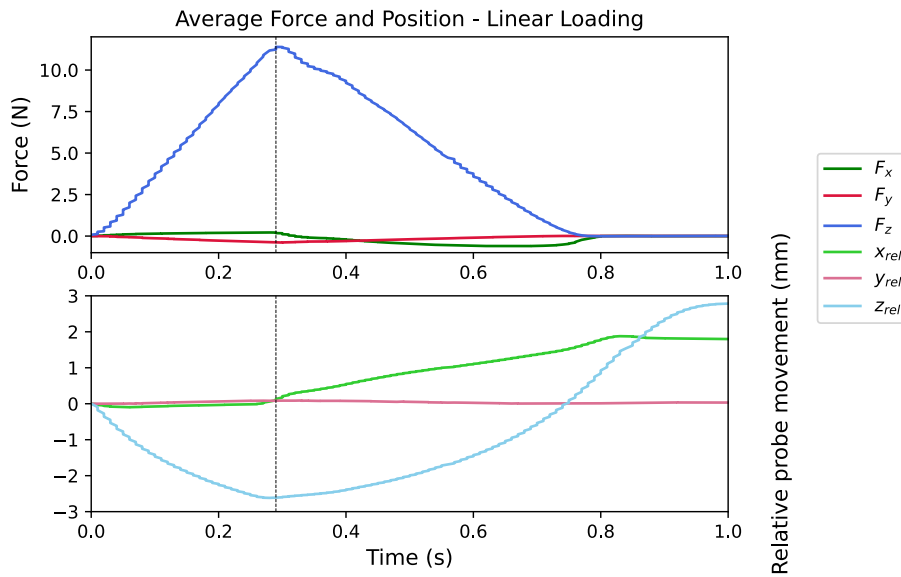


Figure 4.10.: Normal force and relative probe displacement of the experiment depicted in 4.3(b)

Dynamic Cyclic Force Experiments

Requirements. The dynamic experiments demonstrate the required capability to apply normal forces in a cyclic manner. Therefore the sensor is able to test the dynamic response of a sensor. They show that the setup is capable of applying forces that exceed the required force range of 0-10 N. This is useful for testing tactile sensors that require forces greater than 10 N. The experiments also show that the force targets for F_z are exceeded by up to 493 % for a target force of 1N. Furthermore the peaks show a standard deviation of up to 1.7 N between different experiments. This exceeds the force variability requirement of 0.1 %. Thereby the formulated force targets are not met.

The force resolution of 0.03 N is already achieved by the linear normal force experiments. As in the linear force experiments, shear forces are measured. This shows that for this procedure the independent control of normal and shear forces is not achieved.

Analysis. The origin of the shear forces is the same as for the previous discussed linear normal force experiments. However, the issue of the exceeded normal force targets needs to be analyzed. The figure 4.11 shows the average normal force F_z and the relative probe displacement in z direction for the dynamic cycle experiment conducted in 4.4(c).

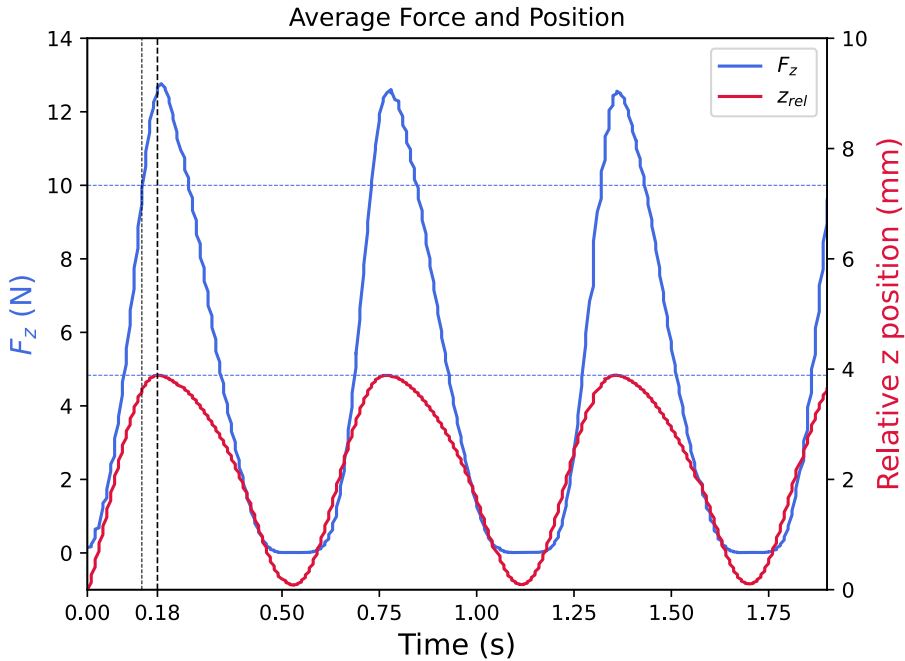


Figure 4.11.: Average probe displacement for the experiment

The blue line depicts that the target force $F_z = 10$ N is reached at approx. $t = 0.14$ s while the red line shows that the peak for the displacement is observed at 0.18s. This reveals that there is a delay of approx 40 ms between detection and reaction to the force.

With a force rate of $\frac{10N}{140ms} = \frac{1}{14} \frac{N}{ms}$ this amounts to an additional force of $F = \frac{1}{14} \frac{N}{ms} \cdot 40ms = 2.85N$. This explains the exceeded target force.

A fraction of this delay stems from the combined delay between the Python-MIOS interface, force sensor and the network in the system that is assumed to be between 10-20ms (). Additionally, the time the robot takes to decelerate is also a factor.

Possible solutions to this might be to add a force prediction that initiates the deceleration process before the force target is reached to avoid overshooting. Additionally, the delay between the system components is possibly minimized by moving the Python implementation onto the realtime PC to minimize the delay through the network.

Quasistatic Experiments

Requirements. The quasistatic force experiments show that static forces can be applied in a cyclic manner for different periods of time. Thereby the static force shows a drift of up to 5.1% of the target force for each of the experiments. The requirements state that the quasistatic procedures require a maximum target force deviation of 1%. This is to ensure that the drift of the tactile sensor can be determined properly without introducing errors through the actuator. The procedure does not meet the requirements. Here, the force F_z shows an average deviation between the experiments of up to 0.25 N. Similarly to the other normal force procedures, shear

forces are applied.

Analysis The reason for the drift this is depicted in figure 4.12. It shows the relative z position of the probe (red) in combination with the normal force (blue). The probe position is considered relative to the point of contact where the probe first touches the sensor surface. The vertical lines depict the respective position and force at the start of the dwell time. Over the cycle duration a shift of both probe position and force is observed. Thereby the red line shows a drift of 0.09 mm.

Once the dwell time is reached, the impedance controller of the robot switches to idle mode. Thereby it is not actively actuating the force on the sensor. An possible origin for the shift of position is the softness of the silicone. After compression, the silicone relaxes and thereby allows the probe to sink in further into the sensor.

One possible solution for this is to not use the idle state of the impedance controller but rather use an active force control during dwell time.

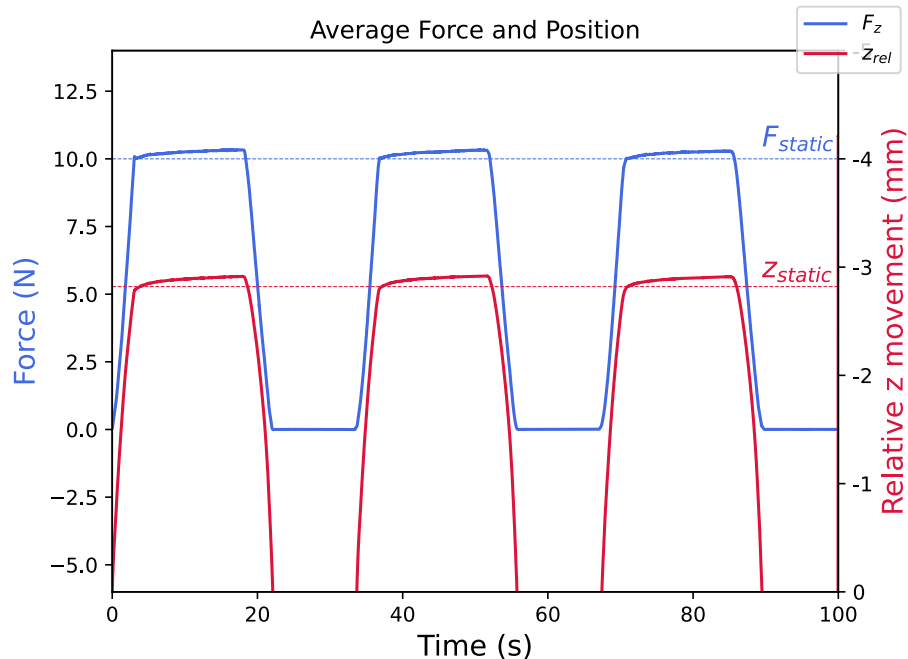


Figure 4.12.: Normal force and relative probe displacement in negative z direction during a quasistatic experiment. The red line indicates a shift of the probe while the static force is applied.

Shear Force XYZ

Requirements. The XYZ shear force experiments show that the experimental setup is capable of applying normal and shear forces independently. This is demonstrated by the experiment results depicted in 4.6(a). Thereby the normal and shear forces are applied as intended. The applied normal force stays constant while the shear force is loaded and deloaded. The force target $F_{shear} = 3\text{N}$ is reached for every experiment variation within a deviation of 0.6%. This concludes that the target force deviation requirement is met for F_y .

However, this is only the case for aforementioned experiment. The other XYZ experiments show a maximum target deviation for F_z of up to 89,9%. This exceeds the target force deviation

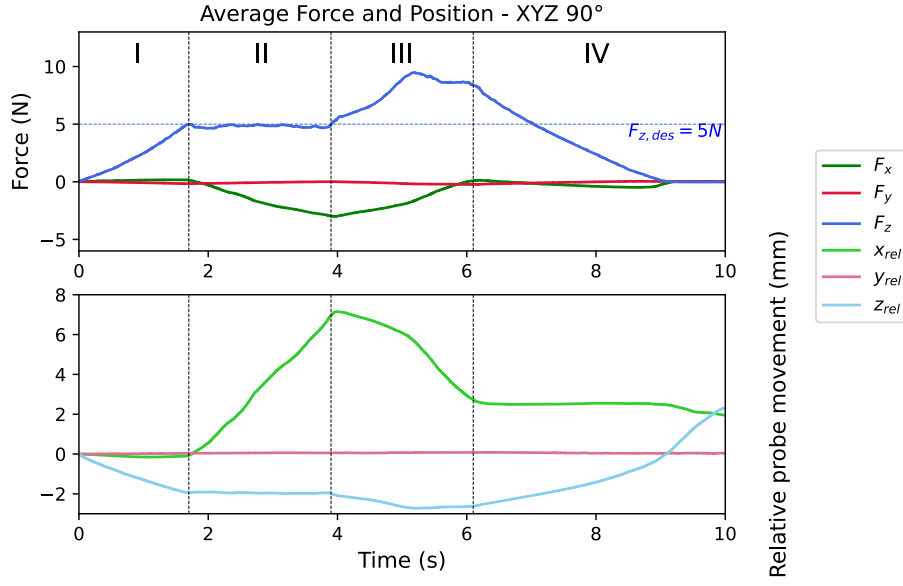


Figure 4.13.: Normal, shear force and relative probe displacement in z direction during the XYZ experiment with 90° . The blue line indicates a shift of the probe in z direction during lateral movement.

requirement for F_z .

Analysis. It is not expected that the actuator behaviour varies based on which direction ($\pm x/y$) the force is pointed to. Based on the experiments conducted with 0° and 180° for XYZ shear force, it is observed that the strong force distortion only occurs for movements involving a component in positive or negative x direction of the robots global coordinate system.

This can be observed in figure 4.14. The upper plot shows the average forces during an XYZ experiment with 90° orientation and a target force of 5N for F_z . The lower plot shows the respective probe movement. The probe position is considered relative to the point of contact where the probe first touches the sensor surface.

- (I) The normal force is applied as expected without any noticeable deviation for x_{rel} and y_{rel} . Thereby z_{rel} decreases as the probe lowers onto the sensor surface.
- (II) The shear force loading phases is initiated. In this phase, x_{rel} increases while z_{rel} stays constant. Thereby the forces F_x and F_z are measured as expected.
- (III) The loading phase is finished and the probe moves back towards negative x direction, indicated by decreasing line for x_{rel} . Here, the unintended movement of the probe in z direction is observed. While the probe is supposed to remain at the same height, the probe is further lowered into the sensor, indicated by the decreasing line for z_{rel} . Thereby the measured normal force increases. At this point in time, the target force of $F_z = 5\text{N}$ is exceeded.
- (IV) Here, the probe stops moving towards negative x direction. At the same time, the probe is lifted from the sensor surface. The final positions of x_{rel} and z_{rel} indicate that the probe does not return to its initial position.

During the whole process, the actuator shows no movement in $\pm y$ direction. Similarly, no shear force F_y is observed.

This behaviour indicates another possible origin for the shear forces measured in the normal force experiments. The figures 4.4 for the dynamic cyclic experiments show a positive force F_x (negative x direction) during loading and a negative force F_x (positive x direction) during unloading. Consequently, it is assumed that every movement in z direction is coupled with a movement in x direction and vice versa. This is depicted in figure 4.14. On the left side, it shows the directions for the different XYZ variations. Indicated in red is the coordinate system of the force sensor. The middle part shows the simplified F_z forces observed for the respective experiments that share a similar movement pattern regarding probe the x direction. The right side depicts the robot and the movement coordinate system as well as the tilting motion that is observed for the end effector.

However, in figure 4.13 (II) no movement in positive z direction is observed despite the motion in x direction. Here, it is assumed that the reason for this is that the probe slides as much downwards of the silicone dome as it is lifted by the tilting motion. Thereby the relative z motion is compensated.

This tilting motion has several possible origins. First, every robot is subject to uncertainties regarding its internal model [TA92]. In our case the robot is controlled through cartesian coordinates. Thereby the inverse kinematics use the internal model of the robot to calculate the respective joint pose. Due to the uncertainties in the model, this leads to errors in the pose estimation and therefore adds to the movement uncertainty.

Furthermore, different joints are utilized for the respective movement in x and y direction. Thereby the end effector position depends on the motion capabilities of each respective joint. Finally, another software related origin is also possible. The stiffness of the robots impedance controller is adaptable to different situations. In this case, the current parameters of the controller are assumed to show an impact on the respective motions.

For these issues, several solutions exist. First, it is possible to replace the current robot and use a different one with a more precise internal model and joint accuracy instead. Second, the motion control is also achievable through joint coordinates.

This removes the need for the internal inverse kinematics and therefore also the errors that result from the internal model. The last solution is to adapt the stiffness parameters of the impedance controller regarding for the different axes and examine if that improves the tilting issue.

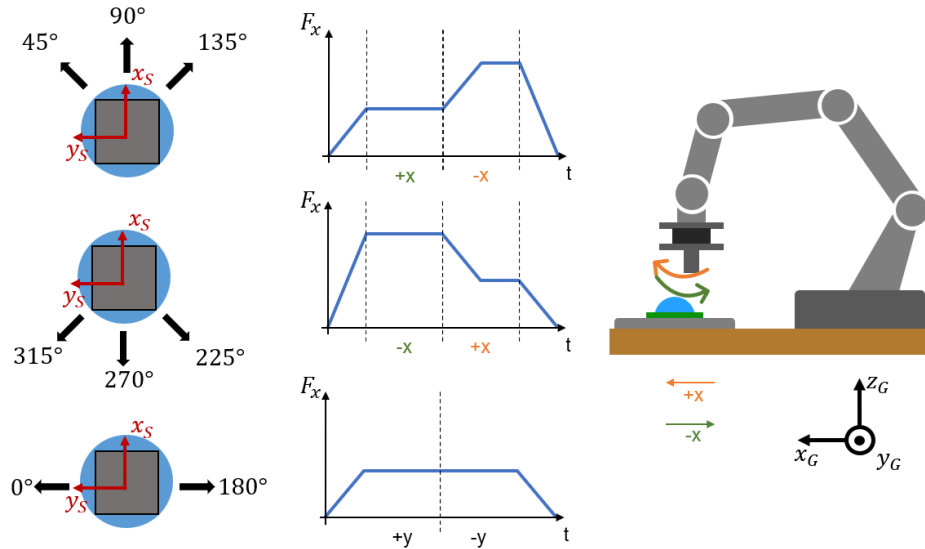


Figure 4.14.: Overview for the depicted behaviour regarding the actuation in positive and negative x direction.

Shear Force XY

Requirements. The results of the XY shear force experiments show that the average maximum shear force is $F_y = 4.92$ N. This results in a deviation regarding the target force $F_y = 5$ N of 1.6 %. Therefore the requirement for the maximum target force deviation is achieved. However, a maximum average deviation between experiments for F_y is measured with 0.37 N. Consequently the requirement for the average deviation threshold between experiments is not achieved. A maximum force of $F_y = 5.47$ N is measured during the experiments. The target forces for the experiments is $F_z, F_x = 0$ N.

Analysis. The tilt movement can also be observed during the XY experiments. Figure 4.15(a) depicts the averages force and relative position for the XY experiment for 270°. The probe position is considered relative to the point of contact where the probe first touches the sensor surface.

(a) This interval shows the beginning of the loading phase for F_y . It is observed that during this interval z_{rel} is rising. This is depicted in the image with Δz_1 . This shows that the probe does not indent the sensor horizontally but with a component in positive z direction.

(b) This interval depicts the deloading phase. However it is observed that while x_{rel} is decreasing, z_{rel} is decreasing as well. Thereby the force F_z rises as the probe pushes further into the sensor while moving downwards. This indicated by the red arrow in image b. This explains why the

(c) & (d) Show the points in time before and after the sensor slides down from the tactile sensor. Thereby it shows the relative displacement Δz_2

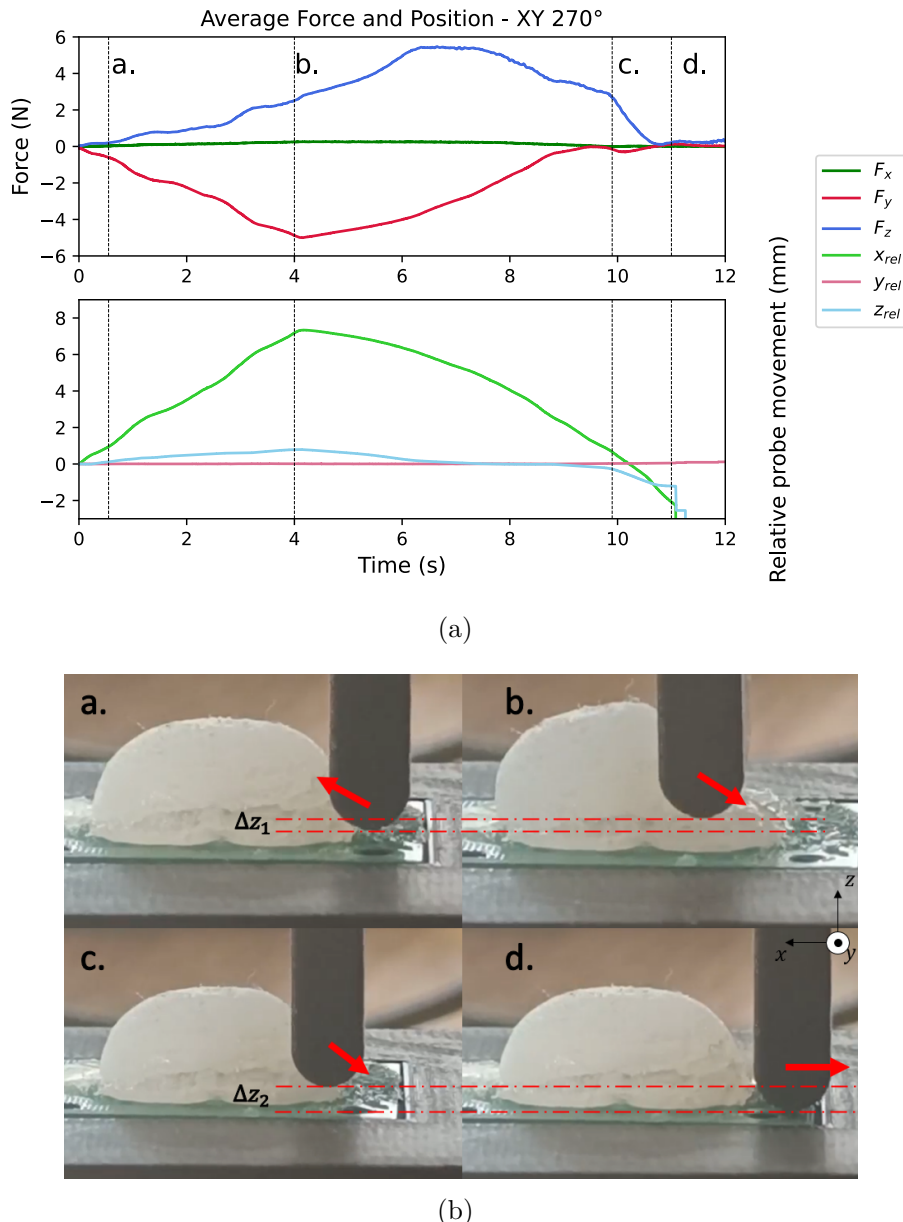


Figure 4.15.: (a) Normal, shear force and relative probe displacement in z direction during a XY experiment with 270°. (b) Image of the sensor during the XY 270° loading process.

Sliding Experiment

Requirements. The sliding experiment demonstrate that the setup is capable of performing a sliding motion on the sensor surface. Thereby the target force $F_z = 1$ N is exceeded by up to 26%. Consequently the requirement for the maximum target deviation threshold is not achieved. The force F_z shows a maximum deviation between experiments of 0.26 N. As a result, the requirement for the requirement for the maximum average deviation is not met. Maximum shear forces of $F_x = 0.57$ N (SD = 0.12 N) and $F_y = -2.99$ N (SD = 0.2 N).

Analysis.

The shear forces observed during the sliding experiments are assumed to be induced from the

tilting related error for motions in z and x direction.

The sliding experiment demonstrate that the setup is capable of performing a sliding motion on the sensor surface. However, this experiment also shows unintended behaviour. The force F_x is caused by the above mentioned path uncertainty for vertical movements. Whereas the additional increase for F_z has a different origin.

Measurement and Structural related Requirements

The K3D40 sensor provides a measurement accuracy of 0.05 to 0.1 N . By itself, the sensor achieves the required measurement accuracy of ≤ 0.1 N. However as depicted in the beginning of the last chapter, the mounting structure introduces a bias for the shear force measurements. This error is not calculated, but it is assumed that the measurement error is above the required measurement accuracy.

The experimental setup provides a user friendly interface that enables executing the experiment parameters through a python script. Thereby no knowledge of the MIOS control system is required to conduct experiments. The operator is able to run every experiment in an automated manner. The end effector design enables the attachment of different probe designs.

Additionally, the setup has two mounting platforms that fit tactile tensors.

5. Conclusion and Outlook

Despite the fact that the designs of modern tactile sensors are based on the same physical principles, the testing methodologies for tactile sensors are not uniform.

To develop an experimental setup capable of characterizing and evaluating different tactile sensor designs, a system concept based on the requirements for tactile sensors in manipulation was developed. Thereby this setup is required to test tactile sensors regarding the measurement of normal force, shear force and vibration using linear, dynamic cyclic and quasistatic cyclic test methodologies. From this, the system requirements are formulated and experiment designs are developed.

The components for the experimental setup are chosen based on the requirements formulated for the system. A Franka Emika Panda robot is utilized as actuator for executing the experiment procedures. To measure reference data for sensor calibration and evaluation, a K3D40 3-axis force sensor is attached to the robot end effector. Thereby it measures the applied forces applied through a attached measuring probe. To attach the sensor to the end effector a mounting structure is designed and 3D printed using PLA material. Additionally, a structure for mounting the tactile sensors are designed and printed.

The developed system is controlled with a layered structure consisting of the motion control system MIOS that drives the robots impedance controller, Python and a Python-MIOS interface. A control system is achieved that enables automated execution of the test methodologies through a command-based Python interface.

In order to examine the developed setup regarding its ability to characterize and evaluate tactile sensors, experiments are conducted. Thereby the force accuracy of the actuator is evaluated in relation to the respective force targets of the test methods. The results are depicted in figure 5.1.

Linear, dynamic cyclic and quasistatic cyclic experiments show a maximum deviation of the target force of 13.9% ($F_t = 10N$), 493% ($F_t = 1N$) and 5.10% ($F_t = 10N$) respectively. In addition to that, unintended shear forces are observed for every normal force experiment. Shear force experiments XY (F_y in xy-plane) and XYZ ($F_{x,y}$ & F_z) show a maximum deviation of the target force of 1.6% ($F_t = 5N$) and 0.6% ($F_{t,x} = 3N$), 0.6% ($F_{t,y} = 3N$) and 89.9% ($F_t = 5N$). A sliding experiment is conducted that shows a maximum deviation of the target force of 26% ($F_t = 1N$)

The discussion reveals that there are two factors that contribute significantly towards the errors in the system.

The first is a delay between recognizing that the target force has been reached and the response to that. Due to this factor, most normal force experiments fail the force tasks because they overshoot their target force.

Modality	Method	Max. Target Deviation ($\leq 10\%$)			Max. Standard Deviation between Experiments ($\leq 0.1 \text{ N}$)		
		F_x	F_y	F_z	F_x	F_y	F_z
Normal Force	Linear	-0.61 N	-0.39 N	13.90% ($F_{target} = 10 \text{ N}$)	0.05 N	0.02 N	0.29 N
	Dynamic Cyclic	-0.61 N	-0.34 N	493% ($F_{target} = 1 \text{ N}$)	0.09 N	0.05 N	1.70 N
	Quasistatic Cyclic	-0.50 N	-0.29 N	5.10% ($F_{target} = 10 \text{ N}$)	0.04 N	0.02 N	0.25 N
Shear Force	XY	0.12 N	1.60 % ($F_{target} = 5 \text{ N}$)	5.47 N	0.03 N	0.23 N	0.30 N
	XYZ	0.60 % ($F_{target} = 3 \text{ N}$)	0.60 % ($F_{target} = 3 \text{ N}$)	89,90 % ($F_{target} = 5 \text{ N}$)	0.08 N	0.08 N	0.34 N
Sliding		0.57 N	-2.99 N	26,00% ($F_{target} = 1 \text{ N}$)	0.12 N	0.20 N	0.26 N

Is actively controlled
Does not meet
requirement

Should be zero
Large in comparison

Is actively controlled
Meets requirement

Should be zero
Small in comparison

Figure 5.1.: Experiment results regarding the formulated requirements for force thresholds.

Secondly, the factor that produces errors in every experiment procedure, is the tilting motion of the robot arm depicted in 4.14. Thereby a motion in both x and z direction of the global coordinate system is executed whenever a procedures involves a movement in the respective directions ($x \leftrightarrow z$, $-x \leftrightarrow -z$).

This factor renders the normal, shear force and sliding experiments unsuitable for sensor calibration. As the forces can not be applied independent of each other, using the current setup for calibration purposes would induce calibration errors due to disturbing forces. In addition to that, a measuring uncertainty of the sensor of 0.05N to 0.1 and a shear force bias for XY experiments of about 0.07N is observed.

Outlook

Next steps should be aimed at optimizing the state of the setup as it is currently not able to execute the experiment procedures within the required thresholds.

Here, removing the two biggest error sources should be the focus. Thereby it should be examined if it is sufficient to improve the robot control or if it is necessary to switch to a different actuation method, as depicted by [Pia+20]. The use of a robot in combination with a linear stage combines the advantages of both actuators into one system.

Future applications may also include testing other sensor designs such as elastic skins. Thereby a different sensor probe and mount could be designed that enable new experiments such as stretching or twisting.

6. References

- [ACP17] Thiago Eustaquio Alves de Oliveira, Ana Maria Cretu, and Emil M. Petriu. “Multimodal Bio-Inspired Tactile Sensing Module for Surface Characterization”. In: *Sensors (Basel, Switzerland)* 17.6 (2017), pp. 3231–3243. ISSN: 14248220. DOI: [10.3390/s17061187](https://doi.org/10.3390/s17061187).
- [BK18] Utku Büyüksahin and Ahmet Kırhı. “A low-cost, human-like, high-resolution, tactile sensor based on optical fibers and an image sensor”. In: *International Journal of Advanced Robotic Systems* 15.4 (2018), pp. 1–13. ISSN: 17298814. DOI: [10.1177/1729881418783631](https://doi.org/10.1177/1729881418783631).
- [Cir+16] A. Cirillo et al. “A conformable force/tactile skin for physical human-robot interaction”. In: *IEEE Robotics and Automation Letters* 1.1 (2016), pp. 41–48. ISSN: 23773766. DOI: [10.1109/LRA.2015.2505061](https://doi.org/10.1109/LRA.2015.2505061).
- [CHP07] Mark Cutkosky, Robert Howe, and William Provancher. “Handbook of Robotics, Chapter 19: Force and Tactile Sensors Chs.” In: *Handbook of Robotics* November (2007), p. 1611. URL: <http://www.springer.com/engineering/robotics/book/978-3-540-30301-5?detailsPage=authorsAndEditors>.
- [DV13] Ravinder S. Dahiya and Maurizio Valle. *Robotic Tactile Sensing*. Vol. 11. 1. Springer Netherlands, 2013. ISBN: 978-94-007-0578-4. DOI: [10.1007/978-94-007-0579-1](https://doi.org/10.1007/978-94-007-0579-1). URL: <http://link.springer.com/10.1007/978-94-007-0579-1>.
- [Dah+10] Ravinder S. Dahiya et al. “Tactile sensing-from humans to humanoids”. In: *IEEE Transactions on Robotics* 26.1 (2010), pp. 1–20. ISSN: 15523098. DOI: [10.1109/TRO.2009.2033627](https://doi.org/10.1109/TRO.2009.2033627).
- [DN04] Javad Dargahi and Siamak Najarian. “Human tactile perception as a standard for artificial tactile sensing - a review”. In: *International Journal of Medical Robotics and Computer Assisted Surgery* 01.01 (2004), p. 23. ISSN: 1478-5951. DOI: [10.1581/mrcas.2004.010109](https://doi.org/10.1581/mrcas.2004.010109).
- [DIN83] DIN Deutsches Institut für Normung. “Manipulating industrial robots – Performance criteria and related test methods”. In: *Berlin: Beuth Verlag GmbH* 2007.2316 (1983), pp. 1–4.
- [DIN97] DIN Deutsches Institut für Normung. “Accuracy (trueness and precision) of measurement methods and results - Part 1 : Generai principles and definitions (ISO 5725-1 : 1994)”. In: *Berlin: Beuth Verlag GmbH* 2218 (1997).
- [Din11] Ralf Dinter. “Fehlerrechnung für Einsteiger - Eine beispielorientierte Einführung für Studierende der TUHH”. In: (2011), pp. 1–18. URL: physnet.uni-hamburg.de/TUHH/Versuchsanleitung%0A/Fehlerrechnung.pdf%0A.
- [Emi17] Franka Emika. *Franka Control Interface*. 2017. URL: <https://frankaemika.github.io/docs/overview.html>. (accessed: 16.03.2022).
- [Emi20] Franka Emika. *Franka Emika Panda Datasheet*. 2020. URL: <https://download.franka.de/Datasheet-EN.pdf>. (accessed: 16.03.2022).
- [Emi22] Franka Emika. *The Franka Emika Panda*. 2022. URL: <https://www.franka.de/robot-system/>. (accessed: 16.03.2022).
- [Fra16] Jacob Fraden. *Handbook of Modern Sensors*. 2016. ISBN: 9783319193021. DOI: [10.1007/978-3-319-19303-8](https://doi.org/10.1007/978-3-319-19303-8).
- [Fra21] Frankx. *The Frankx project*. 2021. URL: <https://github.com/pantor/frankx>. (accessed: 16.03.2022).

- [Fri12] A.E. Fridman. *The Quality of Measurements*. New York, NY: Springer New York, 2012, p. 214. ISBN: 978-1-4614-1477-3. DOI: [10.1007/978-1-4614-1478-0](https://doi.org/10.1007/978-1-4614-1478-0). URL: <http://link.springer.com/10.1007/978-1-4614-1478-0>.
- [GSC20] Antonia Georgopoulou, Tutu Sebastian, and Frank Clemens. “Thermoplastic elastomer composite filaments for strain sensing applications extruded with a fused deposition modelling 3D printer”. In: *Flexible and Printed Electronics* 5.3 (2020). ISSN: 20588585. DOI: [10.1088/2058-8585/ab9a22](https://doi.org/10.1088/2058-8585/ab9a22).
- [Had14] S. Haddadin. “Towards the robotic co-worker”. In: *Springer Tracts in Advanced Robotics* 90 (2014), pp. 195–215. ISSN: 1610742X.
- [Had+08] Sami Haddadin et al. “Collision detection and reaction: A contribution to safe physical human-robot interaction”. In: *2008 IEEE/RSJ International Conference on Intelligent Robots and Systems, IROS* (2008), pp. 3356–3363. DOI: [10.1109/IROS.2008.4650764](https://doi.org/10.1109/IROS.2008.4650764).
- [Har82] Leon D Harmon. “Automated Tactile Sensing”. In: *The International Journal of Robotics Research* 1.2 (1982), pp. 3–32. ISSN: 0278-3649. DOI: [10.1177/027836498200100201](https://doi.org/10.1177/027836498200100201). URL: <http://journals.sagepub.com/doi/10.1177/027836498200100201>.
- [JPL18] Jasper Wollaston James, Nicholas Pestell, and Nathan F. Lepora. “Slip detection with a biomimetic tactile sensor”. In: *IEEE Robotics and Automation Letters* 3.4 (2018), pp. 3340–3346. ISSN: 23773766.
- [Jam+15] Lorenzo Jamone et al. “Highly sensitive soft tactile sensors for an anthropomorphic robotic hand”. In: *IEEE Sensors Journal* 15.8 (2015), pp. 4226–4233. ISSN: 1530437X. DOI: [10.1109/JSEN.2015.2417759](https://doi.org/10.1109/JSEN.2015.2417759).
- [Ji+16] Zhangping Ji et al. “The design and characterization of a flexible tactile sensing array for robot skin”. In: *Sensors (Switzerland)* 16.12 (2016). ISSN: 14248220. DOI: [10.3390/s16122001](https://doi.org/10.3390/s16122001).
- [JF14] Meghan C. Jimenez and Jeremy A. Fishel. “Evaluation of force, vibration and thermal tactile feedback in prosthetic limbs”. In: *IEEE Haptics Symposium, HAPTICS* (2014), pp. 437–441. ISSN: 23247355. DOI: [10.1109/HAPTICS.2014.6775495](https://doi.org/10.1109/HAPTICS.2014.6775495).
- [Kap+15] Zhanat Kappassov et al. “Tactile sensing in dexterous robot hands - Review”. In: *Robotics and Autonomous Systems* 74.A (2015), pp. 195–220.
- [KSA15] Jelizaveta Konstantinova, Agostino Stilli, and Kaspar Althoefer. “Force and proximity fingertip sensor to enhance grasping perception”. In: *IEEE International Conference on Intelligent Robots and Systems* 2015-Decem (2015), pp. 2118–2123. ISSN: 21530866. DOI: [10.1109/IROS.2015.7353659](https://doi.org/10.1109/IROS.2015.7353659).
- [KUK22] KUKA. *KUKA Website*. 2022. URL: <https://www.kuka.com/en-de>. (accessed: 27.12.2021).
- [Lee+08] Hyung Kew Lee et al. “Normal and shear force measurement using a flexible polymer tactile sensor with embedded multiple capacitors”. In: *Journal of Microelectromechanical Systems* 17.4 (2008), pp. 934–942. ISSN: 10577157. DOI: [10.1109/JMEMS.2008.921727](https://doi.org/10.1109/JMEMS.2008.921727).
- [Li+20] Qiang Li et al. “A review of tactile information: Perception and action through touch”. In: *IEEE Transactions on Robotics* 36.6 (2020), pp. 1619–1634. ISSN: 19410468. DOI: [10.1109/TRO.2020.3003230](https://doi.org/10.1109/TRO.2020.3003230).
- [Liu+15] Honghai Liu et al. “Intelligent Robotics and Applications: 8th International Conference, ICIRA 2015 Portsmouth, UK, August 24–27, 2015 Proceedings, Part II”. In: *Lecture Notes in Computer Science (including subseries Lecture Notes in Artificial Intelligence and Lecture Notes in Bioinformatics)* 9245. August (2015), pp. 495–501. ISSN: 16113349. DOI: [10.1007/978-3-319-22876-1](https://doi.org/10.1007/978-3-319-22876-1).
- [LL86] J Loomis and S. Lederman. “Tactual perception”. In: *Handbook of human perception and performance Wiley* (1986), pp. 1–41.

- [MM22a] ME-Meßsysteme. *Assembly Notes, K3D40 3 axis force sensor*. 2022. URL: https://www.me-systeme.de/produkte/sensoren/kxd/k3d/k3d40/anleitungen/k3d40_000_montagehinweis.pdf. (accessed: 16.03.2022).
- [MM22b] ME-Meßsysteme. *High Accuracy Calibration*. 2022. URL: <https://www.me-systeme.de/shop/de/high-accuracy-calibration-3d1>. (accessed: 07.05.2022).
- [MPM07] Antonio Menditto, Marina Patriarca, and Bertil Magnusson. “Understanding the meaning of accuracy, trueness and precision”. In: *Accreditation and Quality Assurance* 12.1 (2007), pp. 45–47. ISSN: 09491775. DOI: [10.1007/s00769-006-0191-z](https://doi.org/10.1007/s00769-006-0191-z).
- [Moh17] Haradhan Mohajan. “Two Criteria for Good Measurements in Research: Validity and Reliability”. In: *Annals of Spiru Haret University* 17.4 (2017), pp. 421–458. URL: <http://www.jstor.org/stable/2393203>.
- [Mor+07] Antonio Morales et al. “An Experiment in the Use of Manipulation Primitives and Tactile Perception for Reactive Grasping”. In: *October* Fig 1 (2007), pp. 1–7. URL: <http://citeserx.ist.psu.edu/viewdoc/download?doi=10.1.1.90.4792&rep=rep1&type=pdf>.
- [Nod+09] K Noda et al. “MEMS on robot applications”. In: *TRANSDUCERS 2009 - 2009 International Solid-State Sensors, Actuators and Microsystems Conference*. IEEE, 2009, pp. 2176–2181. ISBN: 978-1-4244-4190-7. DOI: [10.1109/SENSOR.2009.5285608](https://doi.org/10.1109/SENSOR.2009.5285608). URL: <http://ieeexplore.ieee.org/document/5285608/>.
- [Noh+16] Yohan Noh et al. “Image-based optical miniaturized three-axis force sensor for cardiac catheterization”. In: *IEEE Sensors Journal* 16.22 (2016), pp. 7924–7932. ISSN: 1530437X. DOI: [10.1109/JSEN.2016.2600671](https://doi.org/10.1109/JSEN.2016.2600671).
- [Pia+20] Pedro Piacenza et al. “A Sensorized Multicurved Robot Finger with Data-driven Touch Sensing via Overlapping Light Signals”. In: (2020).
- [PPS12] Ruben D. Ponce Wong, Jonathan D. Posner, and Veronica J. Santos. “Flexible microfluidic normal force sensor skin for tactile feedback”. In: *Sensors and Actuators, A: Physical* 179 (2012), pp. 62–69. ISSN: 09244247. DOI: [10.1016/j.sna.2012.03.023](https://doi.org/10.1016/j.sna.2012.03.023). URL: <http://dx.doi.org/10.1016/j.sna.2012.03.023>.
- [Pru22] Prusa. *Prusa 3D printer*. 2022. URL: <https://www.prusa3d.com/category/original-prusa-i3-mk3s/>. (accessed: 06.05.2022).
- [Reg12] Paul P.L. Regtien. *Sensors for Mechatronics*. Elsevier, 2012, pp. 1–17. ISBN: 9780123914972. DOI: [10.1016/C2011-0-06204-X](https://doi.org/10.1016/C2011-0-06204-X). URL: <https://linkinghub.elsevier.com/retrieve/pii/C2011006204X>.
- [RZM21] Peter Roberts, Mason Zadan, and Carmel Majidi. “Soft Tactile Sensing Skins for Robotics”. In: *Current Robotics Reports* 2.3 (2021), pp. 343–354. DOI: [10.1007/s43154-021-00065-2](https://doi.org/10.1007/s43154-021-00065-2).
- [Rob22] Universal Robots. *UR5e User Manual*. 2022. URL: https://www.universal-robots.com/media/1802778/ur5e-32528_ur_technical_details_.pdf. (accessed: 07.05.2022).
- [Rom+17] Rocco A. Romeo et al. “Slippage detection with piezoresistive tactile sensors”. In: *Sensors (Switzerland)* 17.8 (2017), pp. 1–15. ISSN: 14248220. DOI: [10.3390/s17081844](https://doi.org/10.3390/s17081844).
- [Rom+21] Rocco A. Romeo et al. “Method for Automatic Slippage Detection with Tactile Sensors Embedded in Prosthetic Hands”. In: *IEEE Transactions on Medical Robotics and Bionics* 3.2 (2021), pp. 485–497. ISSN: 25763202. DOI: [10.1109/TMRB.2021.3060032](https://doi.org/10.1109/TMRB.2021.3060032).
- [Sch+10] Matthias Schöpfer et al. “Using a piezo-resistive tactile sensor for detection of incipient slippage”. In: *Joint 41st International Symposium on Robotics and 6th German Conference on Robotics 2010, ISR/ROBOTIK 2010* 1 (2010), pp. 14–20.
- [Su+15] Zhe Su et al. “Force estimation and slip detection/classification for grip control using a biomimetic tactile sensor”. In: *IEEE-RAS International Conference on Humanoid*

- Robots* 2015-Decem (2015), pp. 297–303. ISSN: 21640580. DOI: [10.1109/HUMANOIDS.2015.7363558](https://doi.org/10.1109/HUMANOIDS.2015.7363558).
- [Tes+09] Seiichi Teshigawara et al. “High sensitivity slip sensor using pressure conductive rubber”. In: *Proceedings of IEEE Sensors* (2009), pp. 988–991. DOI: [10.1109/ICSENS.2009.5398213](https://doi.org/10.1109/ICSENS.2009.5398213).
- [TA92] Aleksandar Timcenko and Peter Allen. “Modeling Uncertainties In Robot Motions”. In: (1992), pp. 137–146.
- [Tom+16] Tito Pradhono Tomo et al. “Design and characterization of a three-axis hall effect-based soft skin sensor”. In: *Sensors (Switzerland)* 16.4 (2016). ISSN: 14248220. DOI: [10.3390/s16040491](https://doi.org/10.3390/s16040491).
- [Wan+16] Hongbo Wang et al. “Design methodology for magnetic field-based soft tri-axis tactile sensors”. In: *Sensors (Switzerland)* 16.9 (2016). ISSN: 14248220. DOI: [10.3390/s16091356](https://doi.org/10.3390/s16091356).
- [Wet+09] Nicholas Wettels et al. “Grip control using biomimetic tactile sensing systems”. In: *IEEE/ASME Transactions on Mechatronics* 14.6 (2009), pp. 718–723. ISSN: 10834435. DOI: [10.1109/TMECH.2009.2032686](https://doi.org/10.1109/TMECH.2009.2032686).
- [YSP17] Jianzhu Yin, Veronica J. Santos, and Jonathan D. Posner. “Bioinspired flexible microfluidic shear force sensor skin”. In: *Sensors and Actuators, A: Physical* 264 (2017), pp. 289–297. ISSN: 09244247. DOI: [10.1016/j.sna.2017.08.001](https://doi.org/10.1016/j.sna.2017.08.001).
- [Yin+18] Jianzhu Yin et al. “Measuring Dynamic Shear Force and Vibration with a Bioinspired Tactile Sensor Skin”. In: *IEEE Sensors Journal* 18.9 (2018), pp. 3544–3553. ISSN: 1530437X. DOI: [10.1109/JSEN.2018.2811407](https://doi.org/10.1109/JSEN.2018.2811407).
- [Yua+15] Wenzhen Yuan et al. “Measurement of shear and slip with a GelSight tactile sensor”. In: *Proceedings - IEEE International Conference on Robotics and Automation* 2015-June.June (2015), pp. 304–311. ISSN: 10504729. DOI: [10.1109/ICRA.2015.7139016](https://doi.org/10.1109/ICRA.2015.7139016).
- [Zhu+20] Lingfeng Zhu et al. “Development of fully flexible tactile pressure sensor with bilayer interlaced bumps for robotic grasping applications”. In: *Micromachines* 11.8 (2020). ISSN: 2072666X. DOI: [10.3390/MI11080770](https://doi.org/10.3390/MI11080770).

A. CAD Drawings

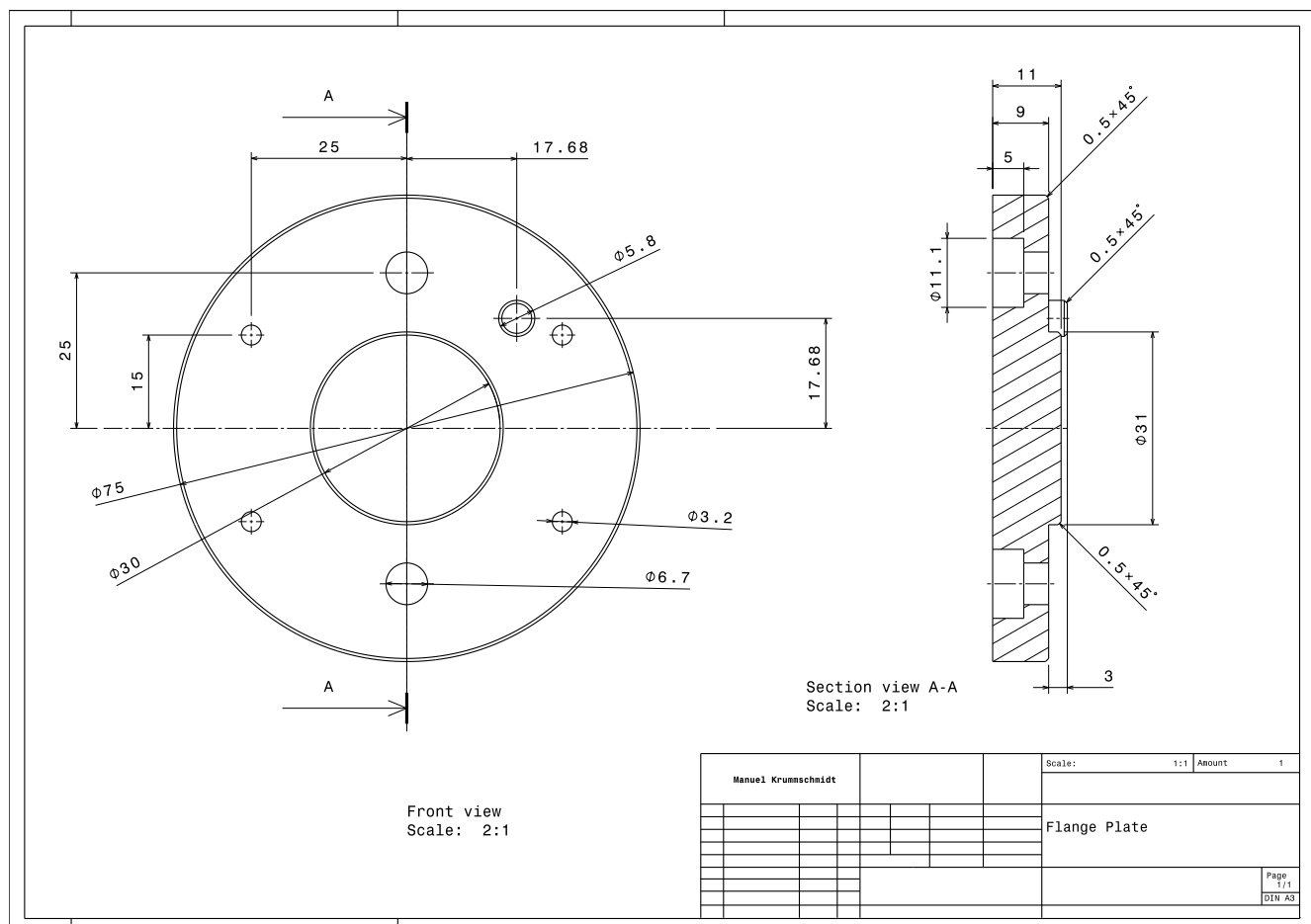


Figure A.1.: The end effector flange plate.

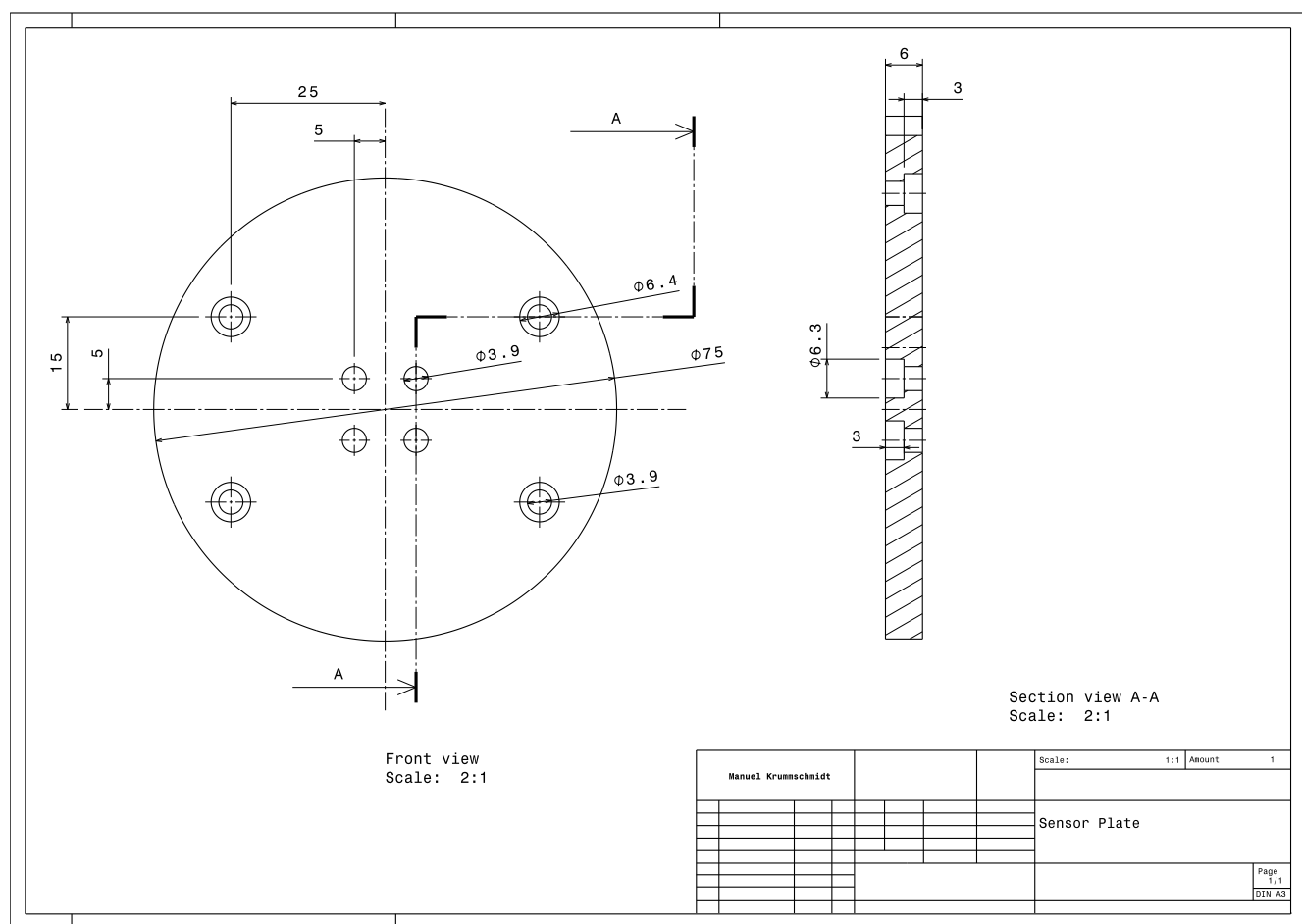


Figure A.2.: The end effector sensor plate.

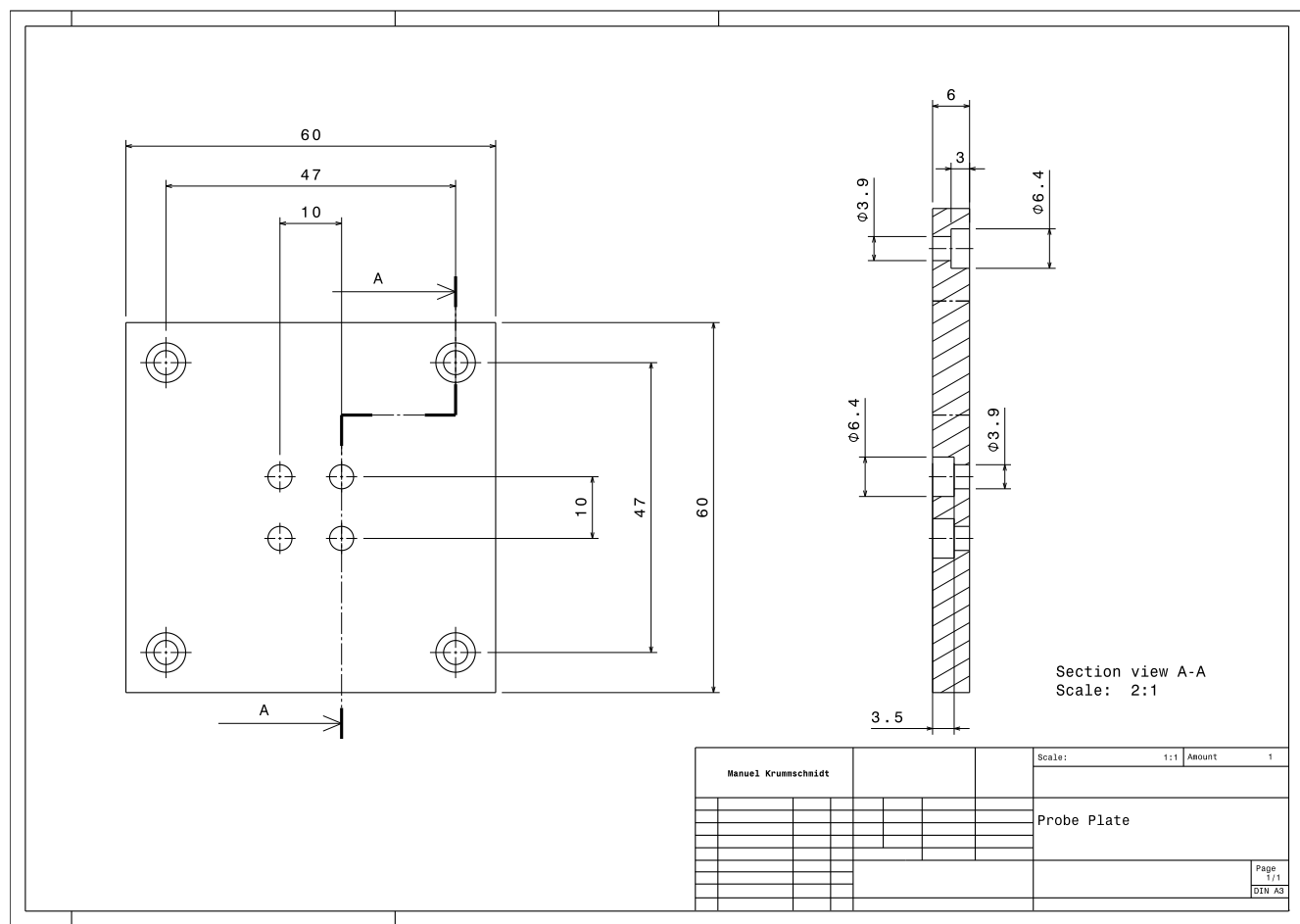


Figure A.3.: The end effector probe plate.

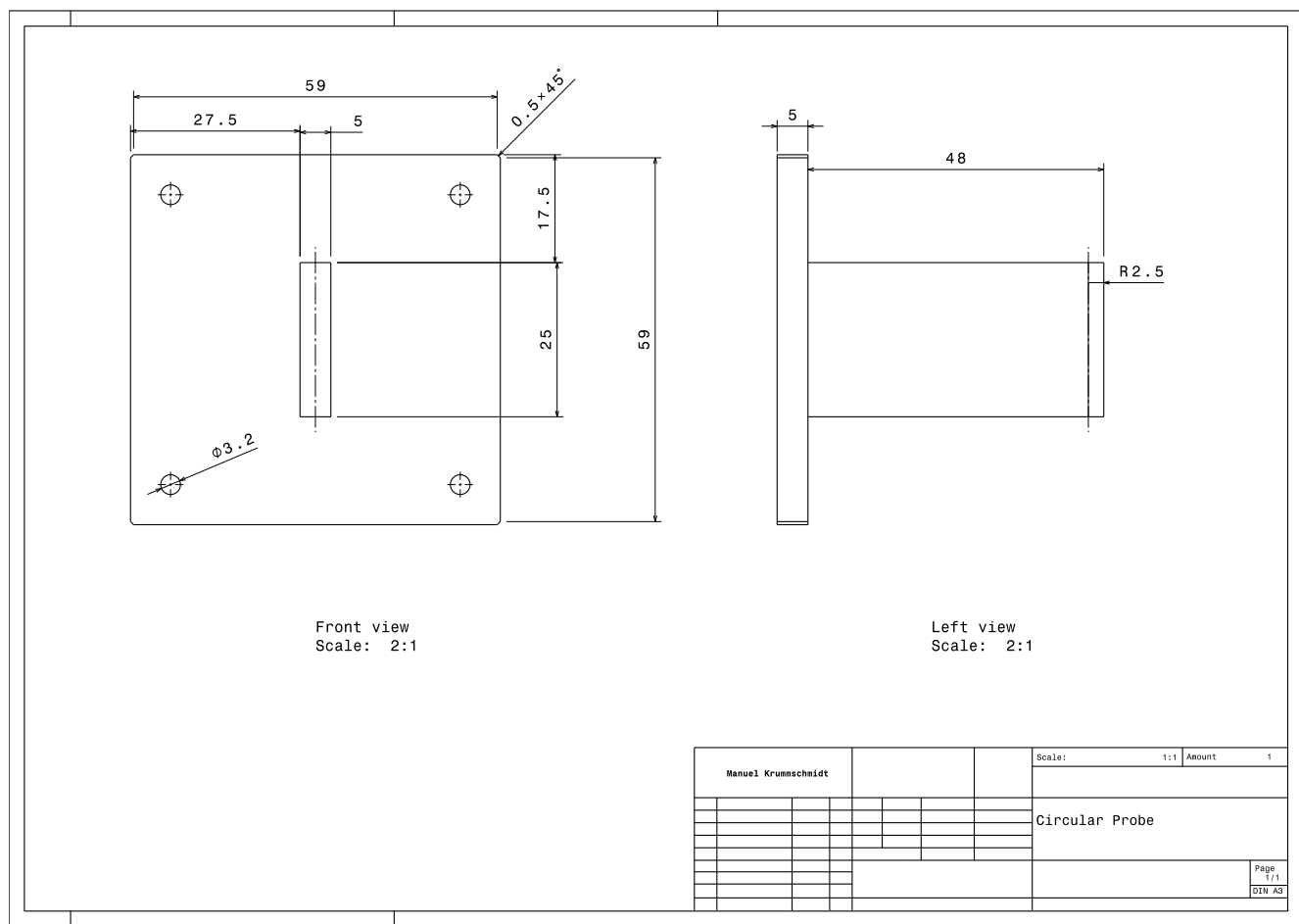


Figure A.4.: The circular probe.

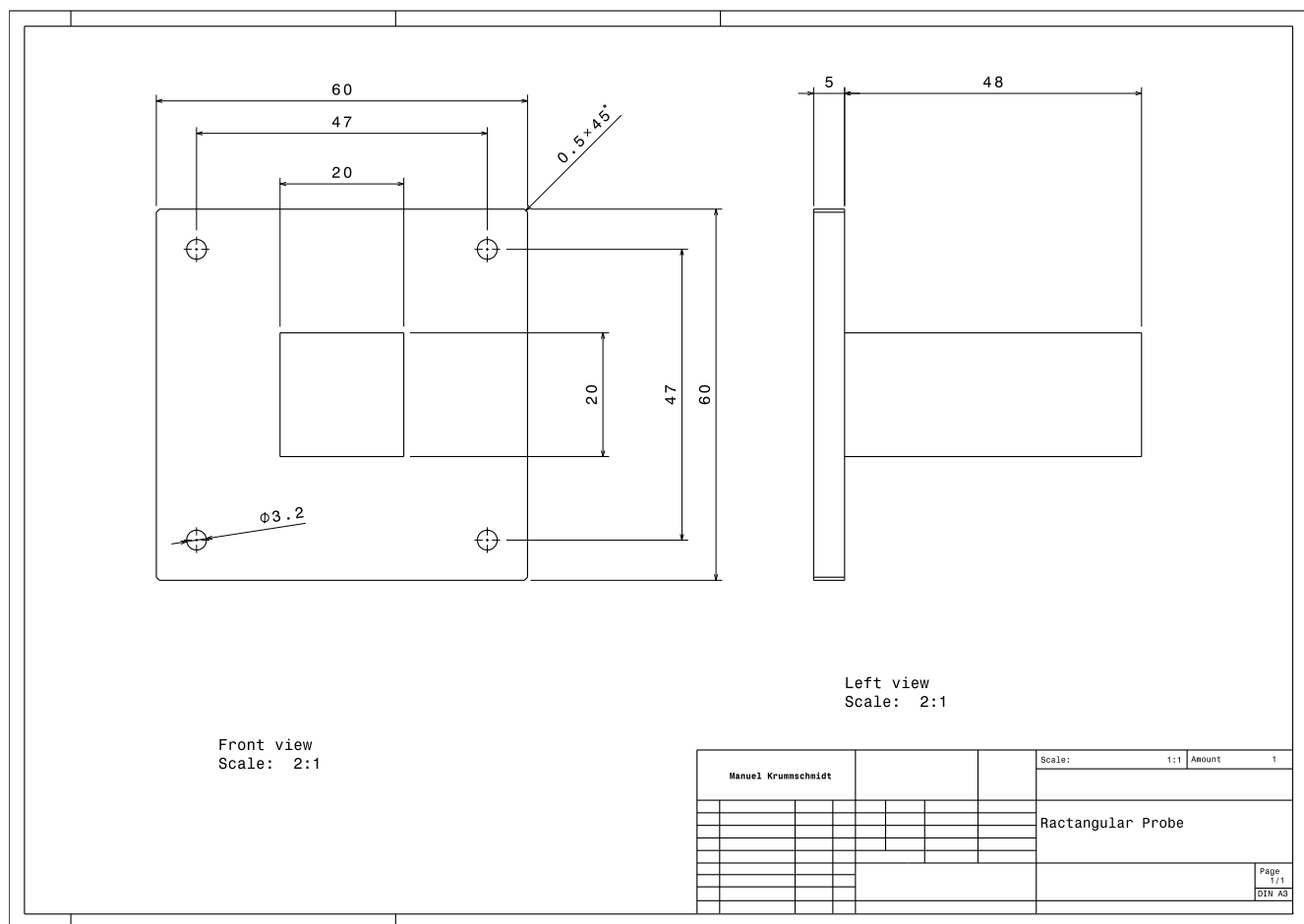


Figure A.5.: The rectangular probe.

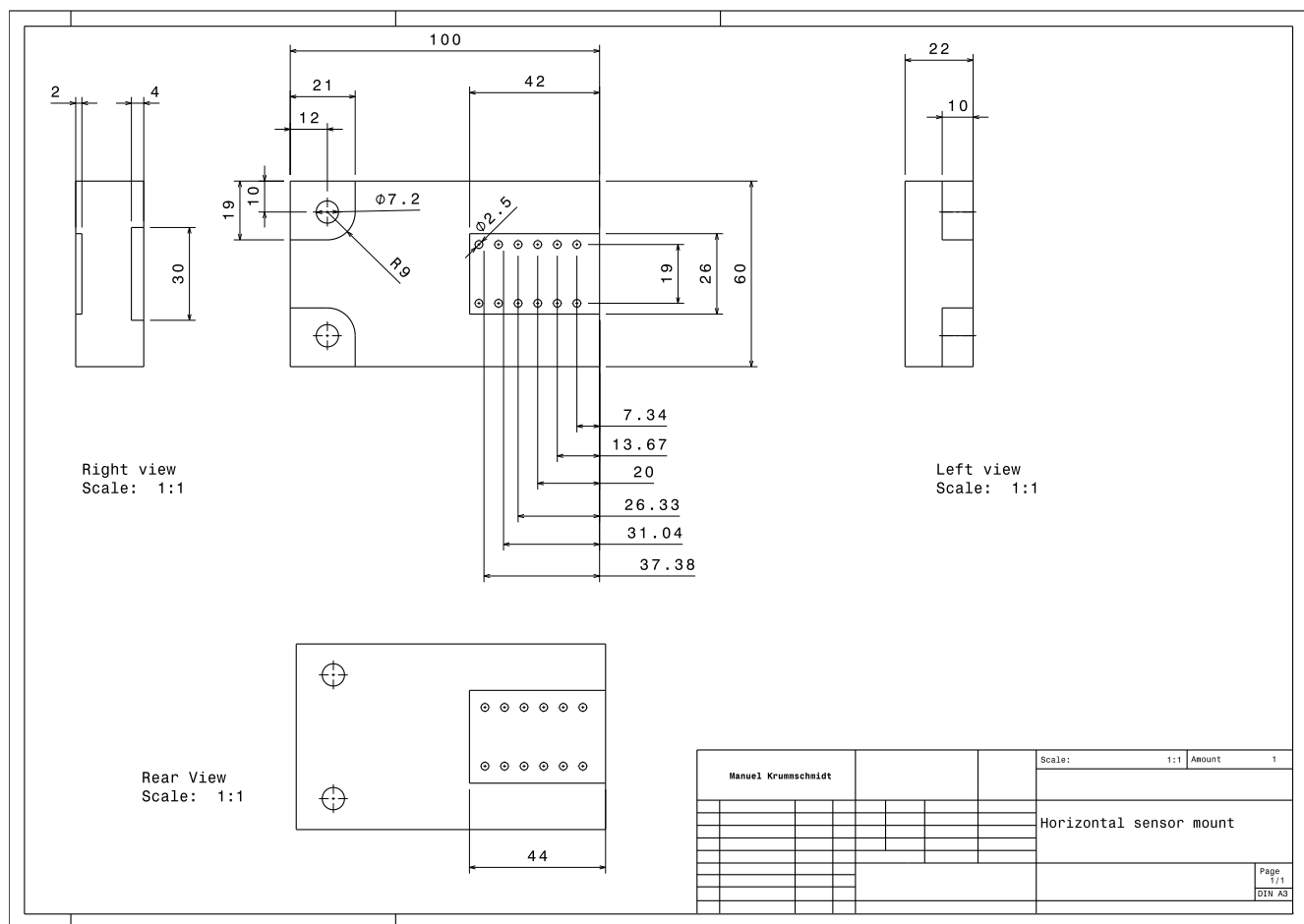


Figure A.6.: The horizontal sensor mount.

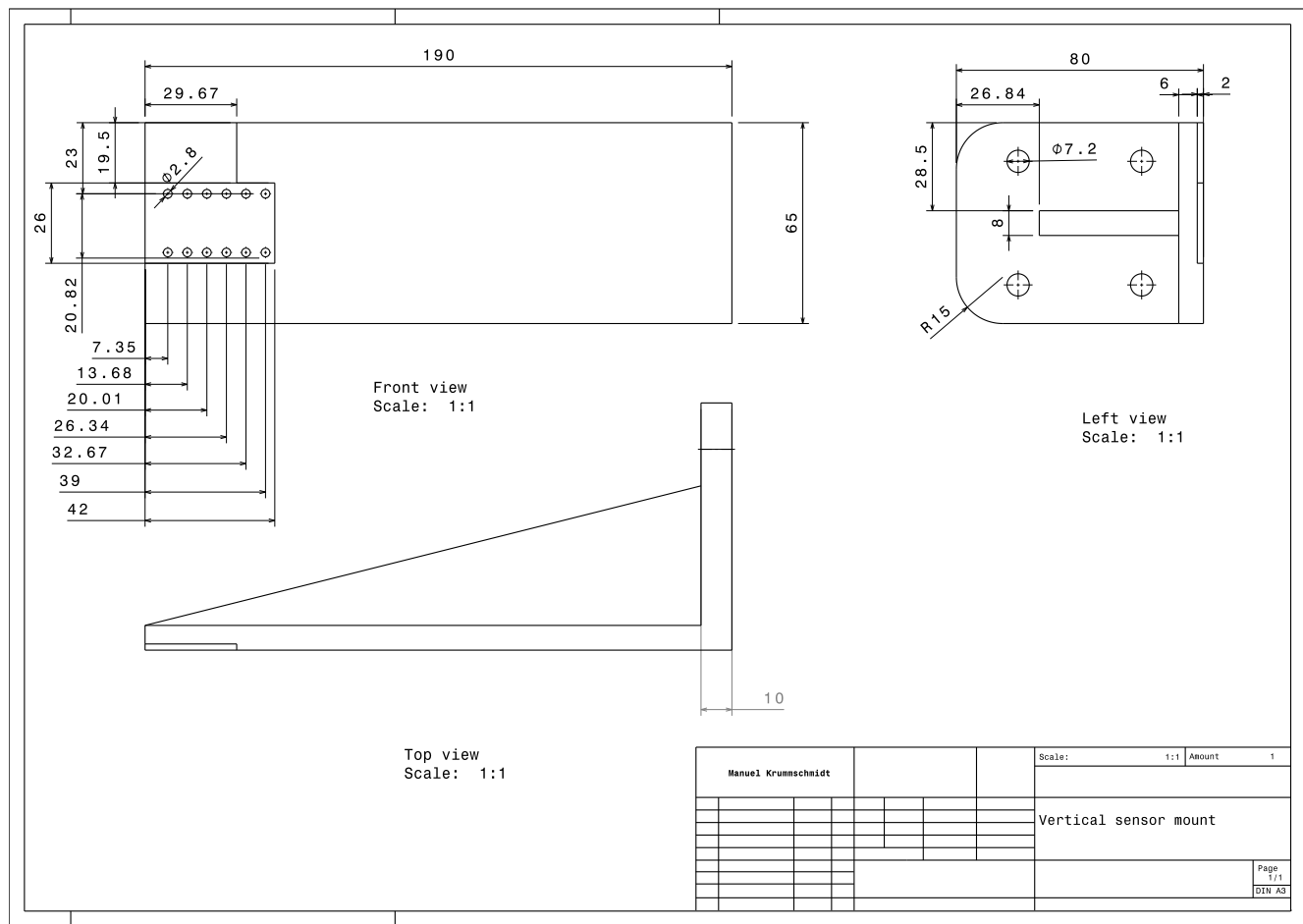


Figure A.7.: The vertical sensor mount.